CENTRO DE INVESTIGACIONES
EN OPTICA, A.C.

“INTELLIGENT ALGORITHMS FOR PROCESSING METROLOGICAL IMAGES”

Thesis submitted in fulfillment of the requirements for the Ph.D. degree in science (Optics)

Presents: Mo. Iosvani Moré Quintero

Advisor: PhD. Francisco Cuevas

León · Guanajuato · México
November de 2021

I would like to dedicate this thesis to the memory of my grandparents and my uncle Enrique, whom with their guidance illuminate my path, blessing me and giving me strength to continue with my goals.

To my parents; including all those who are by choice, whom with their unconditional support, love, and trust allowed me to complete my professional career.

To my little brother and my uncles for their confidence in me, and especially my wife Yaily and children who with their love, patience and effort have allowed me to fulfill one more dream today.

"Before anything else, preparation is the key to success"

Alexander Graham Bell

Acknowledgements

A special thanks to Dr. Francisco Javier Cuevas de la Rosa who as leader of this work has supported, guided, and corrected me in my scientific work.

I am grateful to the thesis committee made up of Dr. Abundio Dávila, Dra. Amalia Martínez, Dra. María del Socorro Hernández, and Dr. Apolinar Muñoz for their valuable contributions during the execution and presentation of the thesis. Their timely comments allowed us to evaluate objectives, propose new ideas, and face the challenges during this work.

I would like to acknowledge the computer resources, technical advice and support provided by Laboratorio Nacional de Supercómputo del Sureste de México, a member of the CONACYT national laboratories, with project No. 201801048n. We also would like to thank the support of the Consejo Nacional de Ciencia y Tecnología de México, and Centro de Investigaciones en Óptica, A.C., that gave me the opportunity to train in the research field and grow professionally and personally.

To all my teachers whom each with their particularities have directly and indirectly influenced my professional training. Additionally, special thanks to PhD. Stephen Jones Barigye for your unconditional support and trust in me.

To my family, friends, and especially those who gave me their unconditional support when I arrived to this country and placed all their hope and confidence in my dream of becoming a professional in science. To my parents, my parents in-laws, and my brother who knew how to support me unconditionally at all times and make my dream theirs. Especially to my wife and children, for being so special that I have no words to thank them and they are my strongest reason for being titled here today

Abstract

In recent years numerous investigations have focused on the problem of fringe pattern demodulation, which has become one of the main challenges in the areas of optical metrology and computer vision. Currently, there is no known method capable of obtaining accurate measurements, especially in transient events with the presence of noise, under-sampling and closed fringes. There are encouraging results through the use of optimization models, such as genetic algorithms, which have demonstrated their efficiency, and, it is a line of research that has gained some momentum in recent decades due to technological progress.

In this work, an investigation of complex fringe pattern recovery using evolutionary computation techniques, in particular the metaheuristics known as Simulated Annealing and Variable Mesh Optimization, is presented. A new system of automatic phase field partitioning of the fringe pattern without overlap, based on the spatial frequency, is introduced, which facilitates the demodulation process, especially in those models that use a polynomial adjustment to approximate the fringe pattern.

Another important aspect presented in this research is the modeling of the objective function using Bézier surfaces as a fitting function, thus generating a novel approach to this type of problems, thanks to the versatility of Bézier surfaces in the area of Computer Vision.

On the other hand, this technique allowed us to characterize and optimize the input parameters of the metaheuristics, as well as to restrict the search space and considerably reduce the demodulation times, which was one of the main challenges of these models using Artificial Intelligence techniques. Finally, the advantage of using Bézier surfaces compared to the use of Zernike polynomials and two-dimensional polynomials reported in the state of the

art is highlighted, and some future works are discussed that may contribute to a substantial improvement of the problem presented here.

Table of contents

List of figures

List of tables

Nomenclature

Greek Symbols

ϕ	phase term which is related to the physical quantity
η	additive noise
π	$\simeq 3.14\ldots$

Superscripts

n	superscript index

Subscripts

0	subscript index
i	subscript index
j	subscript index

Acronyms / Abbreviations

CV	Computer Vision
DIP	Digital Image Processing
FSD	Frequency Guide Sequential Demodulation
FTM	Fourier transform method

HSO Harmony Search Optimization

OM Optical Metrology

OPL Optical Path Length

PLL Phase Lock Loops

PSI Phase shifting interferometry

RPT Regularized phase tracking

SA Simulating Annealing

SLP Structured Light Projection

VMO Variable Mesh Optimization

VR Robot Vision

Chapter 1

Introduction

Over the past few years, a wide variety of technological advances have been achieved that have led to the rapid evolution of optical metrology techniques for 3D surface measurement. Some of these techniques have been used for a long time and have been greatly enhanced with the transformation from screens and photographic plates to digitized intensity patterns. Some others techniques have taken advantage of these new technologies in order to establish new kinds of profilometry measurements, such as confocal microscopy, and time of fly profilometry [2–4].

The developed solutions are traditionally categorized into contact and non-contact techniques. Contact measurement techniques have been used for a long time in reverse engineering and industrial inspections. This type of technique basically has contact with the object of interest, resulting in slow data acquisition and possible damage to the material depending on the strength of the scanner. However, due to the nature of the object of interest to be digitized, this type of technique should be the most feasible.

Non-contact techniques works in such a way that it is not necessary to physically touch the object, using some kind of radiation either emitted by the scanner (active methods), or captured directly from the environment (passive methods).

Among the passive methods are the case of stereo vision, which are generally low-cost setups. However, limited measurement accuracy in depth and computationally intensive digital signal processing requirements reduce their usability in real time profilometric settings [5, 6].

Active methods require laser and/or structured light technology. They can be applied on static objects and require several images to recover the shape or other physical quantities from the digital image. Structured Light Projection (SLP) and Moiré profilometry are examples of this type of method. In Moiré profilometry, mechanical interference is induced by placing a demodulation grating identical but slightly misaligned to the original projection grating between the object and the camera. Contours of equal height can then be extracted from the resulting interference pattern. From a practical perspective, however, the need for a physical demodulation grid complicates the hardware configuration of the experimental setup [7, 8]. More recently, several SLP techniques have been reported that employ the same projector-camera configuration as Moiré techniques, but lack the demodulation grating. Instead, surface height information is extracted directly from the analysis of the deformed grating pattern. By eliminating the demodulation grating, SLP techniques allow designing a simpler and more stable experimental setup. In addition, the extraction of specific depth can be performed in several ways, depending on the nature and amount of projection [9–11].

The development of algorithms in the area of Robot Vision (RV) requires the study, knowledge and understanding of the physics of image formation. Knowing the physics of image formation, we realize that different objects can produce the same two-dimensional images [12–14], which generates ill posed problems, i.e., those in which there is a multiplicity of solutions. In this case, it is necessary to add in the mathematical models a priori information about the objects under study, or to add a greater number of images that describe in more detail and particularize the characteristics of the object, in order to further restrict the solution. In this way, it is possible to limit the solution space to those that most closely match the physical property of the object. Among the main techniques in which it is possible to include a priori information in its mathematical modeling, eliminating those solutions that do not adapt to the previous information are the techniques of Regularized Phase Tracking [15], Evolutionary Computation [16], Neural Networks [17], and in general the Computational Intelligence Algorithms (Soft-computing).

In the areas of Optical Metrology (OM), Computer Vision (CV) and Digital Image Processing (DIP), the problem of recovering physical quantities that are encoded in fringe pattern images

can be classified as a highly complex problem, due to the large number of physical variables involved. Variables such as background illumination, irradiance and reflectance of the object, fringe frequency and additionally the noise generated by the illumination source, as well as the optics and electronics used in the experiment, make mathematical and computational modeling difficult for the calculation of the measurement of physical quantities. Sometimes the object under test may be in motion, increasing the difficulty of the problem. Since it is only possible to obtain an image to perform the quantification of the physical quantity due to the number of physical variables that contribute to the formation of the image, Computational Intelligence techniques are adequate and useful when it is desired to solve ill-posed and highly complex problems.

1.1 Hypothesis

It is possible to model and solve mathematically and computationally, by using Computational Intelligence methods, highly complex problems of OM, improve the reported results, related to the handling of under-sampled images, loss of information in phase images coming from interferometric techniques, structured light projection and pattern recognition.
To this end, the project was broken down into the following specific objectives:

1.2 Objectives

Research, study and develop Computational Intelligence algorithms to solve highly complex problems in the analysis of images generated by the projection, reflection and transmission of structured light to perform 3D reconstruction and pattern recognition in solid, transparent and opaque materials.

To this end, the project was broken down into the following specific objectives:

- ✓ Dynamically adjust windows in structured light images based on their frequency content.
- ✓ Establish window sweeping strategies (sub-images) according to frequency content, using the Quad-tree technique.
- ✓ Model and solve OM problems with subsampled images that do not meet the Nyquist criterion.
- ✓ Comparative analysis of metaheuristics applied to fringe demodulation problems using structured light projection and interferometry.

1.3 Justification

In recent years, a wide variety of technological advances have been developed in digital projection, image manipulation, and processing hardware, which has caused MO techniques for 3D surface measurement to evolve rapidly. The use of fast, high-resolution, non-contact measurement systems has a direct impact on the medical, industrial and entertainment sectors and has motivated manufacturers and academic research groups to design a wide variety of optical profilometry techniques (Optical Profilometry).
In recent years they have worked on intelligent techniques that can solve such problems in an efficient and general way. For this reason, the research line proposed in the project establishes an adequate and feasible technique for three-dimensional reconstruction through the use of Metaheuristics and Intelligent Algorithms.

1.4 Scientific contributions

The main contributions achieved during this thesis project are as follows:

- ✓ Introduction of a novel methodology for three-dimensional reconstruction of objects using Bezier surfaces.

- ✓ Two metaheuristics were introduced to implement the optimization process (RS and VMO)
- ✓ Improvement of the window unification method using spline cubic extrapolation.
- ✓ Application of automatic window partitioning based on frequency content using Quadtree technique.
- ✓ Capability to demodulate small fringe patterns at different resolutions even if it does not meet the Nyquist criterion

1.5 State of the art

Over the past few years, a new group of search and optimization algorithms has been used to solve many real world problems (advanced engineering, data analysis, scientific problems, etc.), which have been formulated as optimization problems [18–20]. Among the areas that stand out is optical engineering, fundamentally optical metrology, which is a non-destructive optical technique used to measure physical quantities such as optical aberrations, deformations, stress,temperature, and the like.

In OM, the reliable measuring of the surface profile of a test object from a fringe pattern is an important problem [21], and generally, a group of optical metrologic techniques such as Interferometry, Digital Holography, Shadow Moire among others, are applied for these measurements [7, 8, 22–36].

In what follows, we present a chronologically ordered review of the research works that have proposed a solution to the problem using soft computing techniques.

Phase Unwrapping by means of Genetic Algorithms [37]:

In February 1998, this article was submitted to J. Opt. Soc. Am., by Antonio Collaro, Giorgio Franceschetti, Francesco Palmieri, and Maria Sedes. It posed the problem of phase unwrapping within a range of $-\pi$ to π. A novel solution was proposed which consisted in performing a randomized path search under a local approach using a genetic algorithm.

Although no computation time is reported, the use of parallel computation is proposed as an alternative, which turned out to be a weakness for this method.

A parametric method applied to phase recovery from fringe pattern base on a Genetic Algorithm [38]:
Published in March 2002 in the journal Optics Communications by F. Cuevas, J.H. Sossa-Azuela, and M. Servin. This article presented the mathematical model that represents the interference phenomenon, which can be formulated as a fringe pattern with a cosine profile:

$$I(x,y) = A(x,y) + B(x,y)\cos(w_x x + w_y y + \phi(x,y)) + \eta(x,y), \tag{1.1}$$

where A represents the background illumination, B the modulation amplitude, w_x and w_y are the carrier frequencies on the respective axes, ϕ is the phase term which is related to the physical quantity and η represents the additive noise.
The demodulation problem was modeled as an optimization problem, whose objective was to recover the term ϕ from the fringe pattern. The objective function used is detailed in Equation 1.2,

$$U(a^p) = \alpha - \sum_{y=1}^{R-1}\sum_{x=1}^{C-1}\Big\{(I_N(x,y) - cos(w_x x + w_y y + f(a^p,x,y)))^2 \tag{1.2}$$
$$+\lambda\left[(f(a^p,x,y) - f(a^p,x-1,y))^2 + (f(a^p,x,y) - f(a^p,x,y-1))^2\right]\Big\}m(x,y),$$

which evaluates the p-esimo chromosome a^p of the population, x and y are the integer values representing the pixel position indices within the interferogram. The superindex p is an integer between 1 and P , which indicates the number of chromosomes or individuals in the population, $I_N(x,y)$ means the normalized irradiance, w_x and w_y are the carrier frequencies, the function $f(:)$ is the fitting function selected to perform the phase approximation, λ represents a smoothing weight factor, and $m(x,y)$ is a binary mask defining the valid area within the fringe pair. The parameter α is used in order to convert the problem from minimization to maximization.

In addition, the possibility of handling different fitting functions was mentioned, although a two-dimensional fourth order polynomial of the form was used:

$$\phi(a,x,y) = a_0 + a_1x + a_2y + a_3xy + a_4x^2 + a_5y^2 + \ldots + a_{\frac{(n+1)(n+2)}{2}-1}y^n. \tag{1.3}$$

Obtaining the phase of an interferogram by use an evolution strategy [39]:
This article was published in June 2002 in the journal Applied Optics Vol. 41 by Sergio Vásquez Montiel, Juan Sánchez Escobar, and Olac Fuentes, it consisted in obtaining the phase of a simulated interferogram with a certain level of noise, finding the wave front aberrations by fixing the coefficients of a polynomial presented as an optimization problem, which was solved by an evolutionary algorithm.
To approximate the phase term a polynomial equation of the type:

$$W(x,y) = A(x^2+y^2) + B(x^2+y^2) + C(x^2+3y^2) + D(x^2+y^2) + E_y + F_y, \tag{1.4}$$

where A is the spherical aberration coefficient, B is the coma coefficient, C is the astigmatism coefficient, D is the defocus coefficient, and E and F represent the tilt in y and x respectively. This function is known as Seidel or Kingslake polynomial for more information it is possible to find it in [40].

Experimental Interferogram analysis using an automatic polynomial fitting method based on evolutionary computation [41]
In April 2005 J. Sanchez and S. Vásquez Montiel published this paper in the Optical Engineering journal, Vol 44. This work proposes a least squares method to obtain the phase in real interferograms. Basically, the proposed method focuses on obtaining the parameters of a polynomial modeled as an optimization problem. Another aspect of relevance is that it performs a comparison between the least-squares method using Z-squared polynomials method using 3rd order Zernike polynomials with an evolutionary algorithm using 3rd order Seidel polynomials.

Window fringe pattern demodulation by multi-functional fitting using a genetic algorithm [42]

In December 2005, F. Cuevas, F. Mendoza, M.Servin, J.H. Sossa-Azuela published this paper in the Optics Communications journal, and introduces a new way of demodulating fringe patterns of higher complexity, which is based on the divide-and-conquer technique, in which the fringe pattern is divided into small, partially overlapping sub-images. As a result of this process there is a lower dimension, which opens the possibility of reducing the time and demodulation is more efficient.

This process is performed sequentially until the entire interferogram is swept. The phase of each sub-image is modeled as an analytical function whose parameters are optimized by means of a genetic algorithm.

Demodulation of Closed Fringe Patterns using a Genetic Algorithm (Master Thesis)[43]:

In December 2005, Otoniel Gonzalez presented a Genetic Algorithm using a cost function defined by Cuevas in [38]. The proposed method has the advantage of working with a single image or with open or closed fringe patterns unlike the Phase Shifting method and the Fourier Transform method, and it does not need a phase unwrapping algorithm because the polynomial approximation finds the phase term directly.

Fast algorithm for phase retrieval of a single interferogram with open and closed fringes (Master Thesis) [44]:

This work was presented in August 2006 by Oscar Dalmau Cedeño and Mariano Rivera. This project presents a two stage algorithm to recover the initial phase using a method based on the use of quadrature filters, it also uses the local orientation information and defines a new entity in the image that will guide the process of formation of the initial phase, the second stage consists of a refinement using Gaussian pyramids.

Among the main advantages reported in the work is a very efficient algorithm from the computational point of view, improving considerably the times in algorithms of the same

type. Good results were obtained both in images with a pattern of open and closed fringes, as well as in synthetic images with a moderate noise level and in real images.

Demodulation of Interferograms of Closed Fringes by Zernike Polynomials using a technique of Soft Computing [45]:
In August 2007, Mancilla, Carpio, and Cuevas published this paper in Engineering Letters, in which introduced a novel way to recover the phase of interferograms of closed fringes by Zernike polynomials using a soft computing technique, applying genetic algorithms (AG) and an optimization fitness function based with Zernike polynomials. The Zernike polynomials are used to obtain the interferogram phase that phase is shown as a surface and due to the orthogonal characteristics of the Zernike polynomials, these are very suitable to carry out the fitting of that surface. By other way, the parameters of the Zernike polynomials have direct relation with the physics properties as: aberration spherical coefficient, come coefficient, astigmatism coefficient, focus shift coefficient, tilt in y, and tilt in x, so on.

Optical Metrology by Fringe Processing on Independent Windows Using a Genetic Algorithm [46]:
Published in January 2008 by Toledo and Cuevas, this paper presents a method to recover the phase map of a fringe pattern based on the demodulation technique per window of a fringe pattern. This method, unlike the one proposed by Cuevas in [42], eliminates the overlap area similarity criterion used in the objective function and replaces it with a second smoothness criterion. This method can measure physical quantities from closed fringe patterns close to the subsampling limit.
The interferogram is divided into a set of partially overlapping windows. In these sub-images the estimated phase is modeled as a parametric function, and its parameters are optimized by a genetic algorithm (GA). This function is used to estimate the phase in the area framed by the window. The phases of all the windows are spliced sequentially to recover the entire phase field. A low-pass filter is applied over the entire phase field. The phases of all windows

are spliced sequentially to recover the entire phase field joints between windows.

A Parametric Method Applied to Phase Recovery from a Fringe Pattern Based on a Particle Swarm Optimization [47]:
This paper was published in December 2011 by J. Jimenez, H. Sossa, F. Cuevas, and L. Gómez. The authors presented a parametric method to carried out fringe pattern demodulation by means of a particle swarm optimization. The phase is approximated by the parametric estimation of an nth-grade polynomial so that no further unwrapping is required. A particle swarm is codified with the parameters of the function that estimates the phase. A fitness function is established to evaluate the particles, which considers: (a) the closeness between the observed fringes and the recovered fringes, (b) the phase smoothness, (c) the prior knowledge of the object as its shape and size.

Frequency guide Sequential Demodulation(FSD)-Harmony Search Optimization (HSO) Algorithm for Closed Fringes Interferogram Demodulation[48]:
This work was presented in March 2016 by U. Rodríguez, M. Mora, J. Muños, and T. Ramírez, introducing a new hybrid mathematical optimization model for phase extraction. The combination of frequency guide sequential demodulation and harmony search optimization algorithms is used for demodulating closed fringes patterns in order to find the phase of interferogram applications.

1.6 Organization of the thesis

The following is a summary of the points developed throughout the document, with the objective of orienting the reader on a specific topic.

Conventional fringe analysis techniques

Chapter 2 gives a brief overview of the main techniques used for interferogram demodulation. It covers in detail the mathematical analysis involved in the determination of the object

topology. In addition, a new approach using intelligent algorithms for the phase demodulation problem will be discussed.

Metaheuristics

Chapter 3 presents the theoretical foundations of the global optimization algorithms that is presented in thesis. Firstly, we start analyzing the operation and modeling of the metaheuristic known as Simulated Annealing, and in a similar way we refer to the optimization algorithm named Variable Mesh Optimization. This chapter will provide the reader with the necessary concepts to be able to implement and understand the used metaheuristics.

Parallel methods applied to fringe pattern demodulating

Chapter 4 is dedicated to the development of the mathematical model used for the adjustment of the object topology. Among the main aspects that we are dealing with will be related to the fitting function, solution coding, solution space, among other details.

Experimental Results

Chapter 5 presents different experimental tests, both with simulated and computer-generated fringe patterns. A comparison of the results with some techniques reported in the state of the art is made, highlighting some of the potentialities of the presented project.

Conclusions and future work

This chapter shows the contributions and proposals for future work supported by the results, giving the reader a perspective of the main lines of research related to the thesis project.

Chapter 2

Conventional fringe analysis techniques

2.1 Introduction

In MO, optical interferometers are generally used to measure a wide range of physical quantities. Depending on the application, different types of interferometers may be used, but their common goal is to produce a fringe pattern where the phase is modulated by the measured physical quantity. Interferometric methods allow us to measure the shape of an optical surface with high accuracy, using wavelength as a measure of length.

There are different techniques to approximate the phase term, among them: electronic and analytical. The tools to obtain the phase electronically are characterized by the use of special hardware, such as zero crossing detector circuits, phase lock loops (PLL) and counters (up-down), used to monitor current data on the interferograms.[49]. On the other hand, analytical techniques are characterized by being digitally captured to be processed by any type of computational algorithm, currently this type of technique is widely used for phase term recovery.

The great technological progress in image processing and acquisition has brought with it the development of interferometric metrology, as well as an increase in phase extraction algorithms, among the best known of which are the Fourier Transform method [50, 51], and the phase shift algorithm [52, 53]. Based on this motivation, the main objective of this chapter

is to present an overview of the interference phenomenon, as well as the main interferometric techniques used in phase field recovery.

2.2 Interference Pattern

The formation of an image relies on the complex interplay between two critical optical phenomena: diffraction and interference. Light passing through the specimen is scattered and diffracted into divergent waves by tiny details and features present in the specimen. Some of the divergent light scattered by the specimen is captured by the objective and focused onto the intermediate image plane, where the superimposed light waves are recombined or summed through the process of interference to produce a magnified image of the specimen. Basically, wave interference is the phenomenon that occurs when two coherent waves are traveling through the same medium with the same frequency and wavelength, and must not exceed the allowed optical path length (OPL) [54, 40].

Among the best known interferometers is the Michelson interferometer, where the amplitude of the incident light field is divided by a beam splitter to split the light from a coherent light source into two beams which are directed through two different pathways to a single detector where the two light waves are recombined producing an interference pattern. The distance between the fringes in the interference pattern can be used to measure very small displacements and distances such as the different lengths of the two light paths or very short time differences. Figure 2.1 shows a scheme of the interferometer configuration.

In practice the light source emits a coherent beam of white light which is split by a half silvered mirror into two separate paths perpendicular to eachother. These two light beams impinge on two further mirrors (1 and 2), at right angles to each other and are reflected back through the beam splitter which recombines them into a single beam and directs the beam into a detector.

Based on the interference phenomenon [54], a fringe pattern can be considered as a fluctuation of a cosinusoidal signal in bidimensional space. Fringe pattern analysis refers to the complete recovery of the original characteristics of a fringe pattern. In this process the only measurable

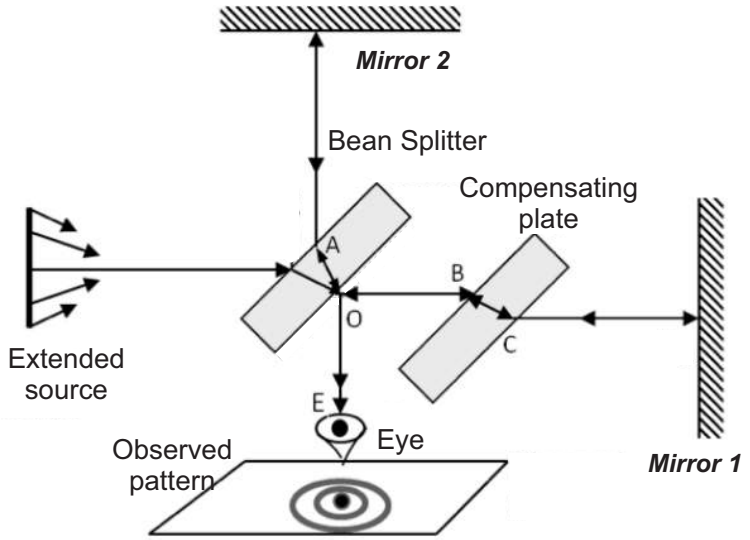

Fig. 2.1 Michelson interferometer.

quantity is the intensity $I(x,y)$, which can be represented through its cosine profile as:

$$I(x,y) = a(x,y) + b(x,y)cos(w_x x + w_y y + \phi(x,y)) + n(x,y), \tag{2.1}$$

where the term $a(x,y)$ represents the background illumination, $b(x,y)$ the contrast or modulation of the signal, w_x and w_y the carrier frequency on the corresponding axes, $\phi(x,y)$ symbolizes the phase term which is linked to the physical quantity to be quantified, and $n(x,y)$ represents additive noise which is added to the relevant signal during capture or transmission [55–57].

Fringe pattern analysis refers to the complete recovery of the original characteristics of a fringe pattern. In recent years, this topic has become a field of application in digital signal (or image) processing. Being a problem related to digital image processing, it is not exempt from the challenges of this branch, i.e., the phase recovery problem is categorized as an ill-posed problem, which is why it is necessary to establish certain conditions to obtain a unique solution. Among the main difficulties that we can find:

1. Ambiguity of the phase in 2π, due to the cosine periodicity.

2. Ambiguity of the sign, due to the parity of cosine.

3. In real cases, the presence of some kind of noise.

2.3 Structured light

With modern advancements in computational methods, optics, and graphics computing, 3D scanning is rapidly becoming more prevalently adopted in society. Among the most popular are structured light scanning system, which represents an extension of the one-point projection technique.

Among the best known methods is the fringe projection method, which has the advantage that in some techniques only a single image is needed to carry out an adequate reconstruction of the object. It also has the advantage that objects of different dimensions can be measured by modifying the frequency of the fringes [58, 59].

The relationship between the phase and the intensity observed in a cosine profile pattern can be approximated by the following expression:

$$I(x,y) = a(x,y) + b(x,y)cos(\varphi(x,y)), \tag{2.2}$$

where $a(x,y)$ describes the background illumination, $b(x,y)$ represents the reflectance variations of the object, and $\varphi(x,y)$ is given by:

$$\varphi(x,y) = 2\pi f_0(x,y) + \phi(x,y), \tag{2.3}$$

where f_0 corresponds to the spatial frequency of the carrier signal, and $\phi(x,y)$ is the associated phase term, which will be used to approximate the shape of the object.

Considering the case where the optical axes of the grating and the camera are parallel along the z-axis (Figure 2.2), where the x and y axes are horizontal and vertical to the reference plane $(z = 0)$, respectively. The projected grating lines are also parallel to the reference plane. The pupil centers of the projector P and the camera C are located at a distance d_0 from the reference plane and are located on the same z-position. By placing an object on the reference plane, the depth of the object can be calculated using the phase extraction

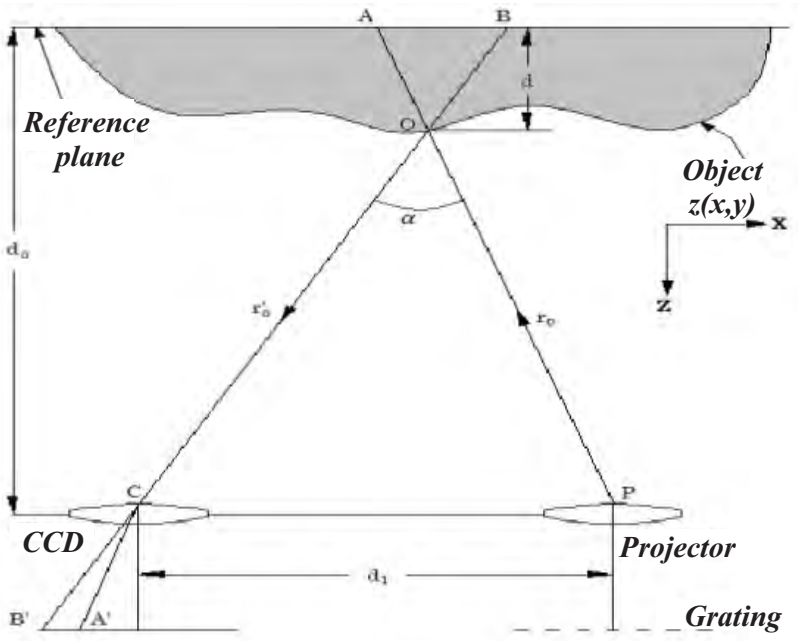

Fig. 2.2 Geometry of fringe projection.

techniques mentioned above. If the distance d_0 is relatively large with respect to d_1, then the grating projected onto the object will be irregular with frequency changes in the x direction, in which case the phase observed at $O(\phi_O)$ will be very similar to the phase at $A(\phi_A)$ and points O and B on the object will be projected onto the image plane at the same point $B^{'}$. The distance $\overline{AB}$ can then be expressed as:

$$\overline{AB} = \frac{\phi_A - \phi_O}{2\pi f}, \tag{2.4}$$

where f is the spatial frequency of the grating over the reference plane and ϕ_B is the phase at point B. In equation 2.4, it can be seen that the distance $\overline{AB}$ is proportional to the phase difference produced by the presence of the object. By analyzing the triangles PCO and ABO in Figure 2.2, we obtain the relation:

$$z(x,y) = \frac{\overline{AB} \cdot d_0}{d_1 + \overline{AB}}. \tag{2.5}$$

After a mathematical expansion, and assuming that the period of the projected grating as $p = 1/f$ and $\Delta\phi = \phi_B - \phi_0$, we can express the above equation as a function of the angle α between the projector and the camera as:

$$z(x,y) = \frac{\Delta\phi(x,y)}{2\pi}\frac{p}{sin\alpha}. \tag{2.6}$$

When the projected fringes with period p are viewed at an angle α have a spacing d perpendicular to the viewing direction given by:

$$d = \frac{p}{cos\alpha}. \tag{2.7}$$

Assuming normal view, the height of the object above the reference plane will be:

$$z(x,y) = \frac{\Delta\phi(x,y)}{2\pi}\frac{p}{sin\alpha} = \frac{\Delta\phi(x,y)}{2\pi}\frac{d}{tan\alpha}. \tag{2.8}$$

It should be noted that if the pattern is generated synthetically by software, the period p must still undergo a transformation from image coordinates to world coordinates, this task can be accomplished by a proper calibration of the projector camera system.

2.4 Shadow moire method

The moire effect is composed of a set of optical techniques that allow the three-dimensional digitization of the topography of a surface. Obtaining the three-dimensional shape of an object has several applications in various areas such as: in medicine for the manufacture of prostheses and diagnosis of diseases; in archeology for digital preservation or reconstruction of archaeological pieces.

This effect occurs when the interference of two gratings that are related at an angle or have different sizes is perceived. In other words, it occurs when two distinct patterns or shapes are superimposed on each other to form a visual effect. Moire techniques go back many years,

and although there are many different moire methods, one of the best known is the Shadow moire technique.

2.4.1 Shadow moire

Shadow Moire technique was applied for the first time by Weller and Shepherd, who placed a grid in front of an object, this to determine its shape, they observed that moire's stripes were visible on it [52].

Shadow moire technique uses a single grid, which is illuminated in front of the object, producing a shadow on it known as moire fringes due to the superposition of the grid and its shadow on the object. This fringe pattern represents the out-of-plane elevation of the surface and is essentially a contour map of the object under study.

To explain moire's shadow phenomenon, it is necessary to consider the following arrangement shown in Figure 2.3 which corresponds to a profile of the object which is obtained by making a cross section of the object. It is considered a source whose rays form an angle α with the optical axis, the lighting creates a shadow of the grid on the surface of the object, the shadow of the grid is represented by a line segment which lengthens when incident on the surface, the elongation depends on the inclination of the surface of the object, the angle of incidence α and the distance from the grating to the object.

2.5 Fringe analysis methods

Many techniques have been employed for analytical phase retrieval, among these are temporal phase measurement methods, which use more than one interferogram, methods based on pixel intensity analysis using numerical interpolation techniques, and those based on spatial phase measurement among which the best known are the phase shifting method [40], the Fourier Takeda method [50, 51], and the regularized phase tracking system [15].

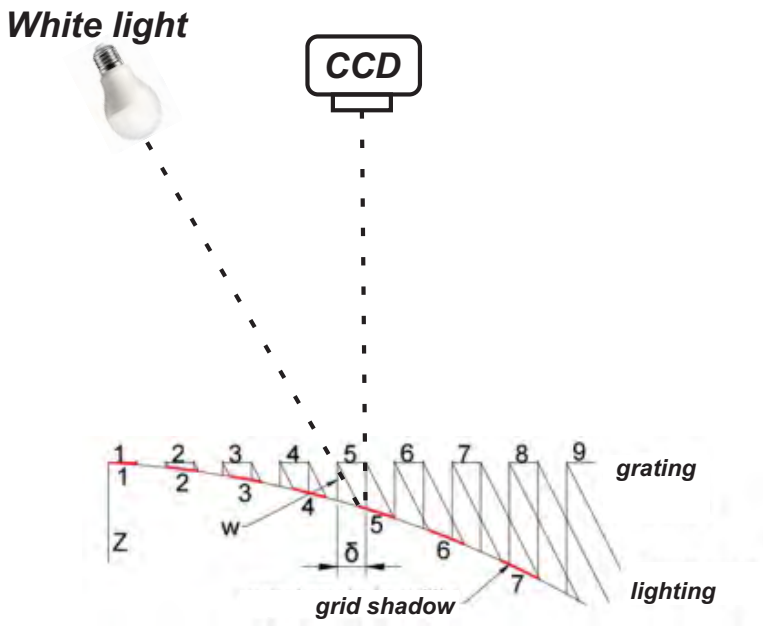

Fig. 2.3 Optical arrangement used in the Shadow moire technique.

2.5.1 Phase shifting interferometry (PSI)

The development of this technique dates back to the work of Carre [60]; later work appeared with Crane [61], Brunning et al. [62], Hardy et al. [63], Brunning [64], and Malacara [40]. Many optical interferometers use this technique because PSI provides a highly accurate, rapid way of getting the interferogram information into a computer. Actually, PSI techniques have been developed allowing the study of static [65, 52] and transient events by employing systems that allow the capture of several interferograms simultaneously retrieving optical phase variation instantaneously [66–68].

PSI is one of the most popular techniques among those that require multiple images to obtain the phase map. Conventionally, this method generates phase shifts by stages, that is, N images are obtained. By means of the generated interferograms, the optical phase can be calculated to be associated later with the physical parameters of the sample under study. To better understand the process, an example of a conceptually and analytically simple algorithm of the variant popularly known as the 4-step method is shown below.

Four step method

The four-step method, as the name implies, requires four interferograms that are totally independent of the object under test; the interferograms must be recorded or digitized. An optical phase shift of $\frac{\pi}{2}$ is introduced into the reference beam between each sequentially recorded interferogram.

Assuming that the irradiance values I_i are measured from their initial value $\phi(x,y)$ and increased by a constant amount δ_i, we have that:

$$I_i(x,y) = a(x,y) + b(x,y)cos(\phi(x,y) + i\delta_i) \qquad i \in [0..N-1], \tag{2.9}$$

where N indicates the number of fringe patterns to be acquired. For the number of samples equal to N, the phase increment is given by the following expression:

$$\delta_i = \frac{2\pi}{N}\ . \tag{2.10}$$

Basically, the larger the number of samples, the lower the level of random noise, which decreases by a factor $\frac{1}{\sqrt{N}}$, although in practice the most commonly used sample number for the phase shift method is $N = 4$, which results in a phase shift of $\delta_i = \frac{\pi}{2}$.

Substituting the values in equation 1.3 we obtain 4 equations describing the intensity patterns of the measured interferograms:

$$I_1(x,y) = a(x,y) + b(x,y)cos(\phi(x,y)), \tag{2.11}$$

$$I_2(x,y) = a(x,y) + b(x,y)cos(\phi(x,y) + \frac{\pi}{2}), \tag{2.12}$$

$$I_3(x,y) = a(x,y) + b(x,y)cos(\phi(x,y) + \pi), \tag{2.13}$$

$$I_4(x,y) = a(x,y) + b(x,y)cos(\phi(x,y) + \frac{3\pi}{2}). \tag{2.14}$$

Solving algebraically the above system of equations, we can conclude that the phase term can be obtained from the following expression:

$$\phi(x,y) = tan^{-1}\left[\frac{I_2(x,y) - I_4(x,y)}{I_1(x,y) - I_3(x,y)}\right]. \tag{2.15}$$

The advantage of this method is that it is based on pixel-level operations which does not sacrifice spatial resolution and the accuracy of the computation can be improved by increasing the number of fringes. On the other hand, like other techniques, this method requires a phase unwrapping algorithm because the object profilometry involves a trigonometric function.

2.5.2 Fourier interferometry

The Fourier fringe demodulation technique, initially developed for the analysis of spatial carrier fringes, was proposed and experimentally demonstrated in the early 1980s [50, 51].The use of this type of spatial analysis techniques has become very popular in recent years, especially in fringe analysis, because phase information can be obtained from a single image. In this epigraph we will focus on the technique known as the Fourier transform method for fringe analysis (FTM).

Fourier transform method

We will begin with a brief description of the theoretical principles of FTM, whose objective is to recover the phase function in the spatial frequency plane. The type of fringe pattern is similar to the fundamental equation describing a fringe pattern in most optical tests, with the only difference being the introduction of a spatial carrier frequency f_0 which is set by tilting one of the interfering beams, as shown in the following equation:

$$g(x,y) = a(x,y) + c(x,y)exp(2\pi f_0 x) + c^*(x,y)exp(-2\pi f_0 x), \tag{2.16}$$

where

$$c(x,y) = \frac{1}{2} b(x,y) exp(i\phi(x,y)), \tag{2.17}$$

and $c^*(x,y)$ represents the complex conjugate.

Applying the fast Fourier transform to Equation 2.16 with respect to x we obtain:

$$G(x,y) = A(f,y) + C(f - f_0, y) + C^*(f + f_0, y), \tag{2.18}$$

where the capital letters denote the Fourier spectrum, and f is the spatial frequency in the x direction. The three spectra in Equation 2.18 are separated from each other by the spatial carrier frequency as shown in Figure 2.4a. Using either of the two spectra on the carrier $C(f - f_0, y)$, and moving it on the frequency axis towards the origin we obtain $C(f,y)$ as shown in the Figure 2.4b.

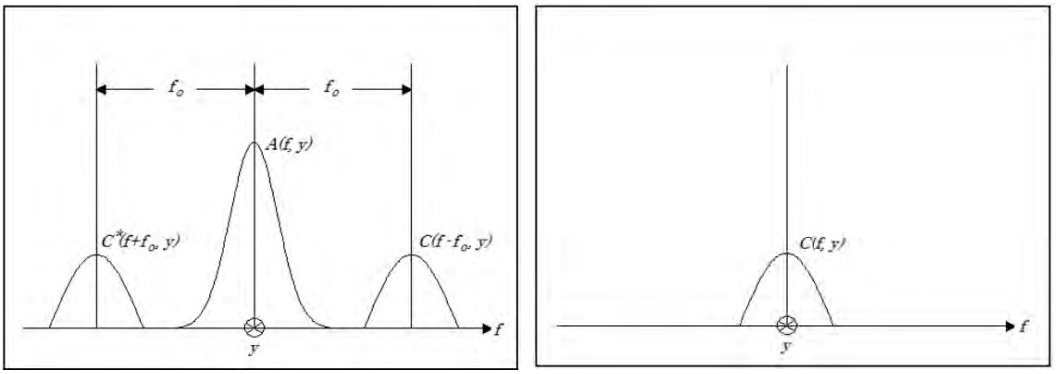

(a) Fourier spectrum. (b) Fourier spectrum shifted to origin.

Fig. 2.4 Fourier spectra of an interferogram.

On the other hand, it can be seen that the background variations $a(x,y)$ have been filtered out at this stage. We now compute the inverse Fourier transform for the $C(f,y)$ term with respect to f, obtaining $c(x,y)$ defined in Equation 2.17. Computing a complex logarithm of Equation 2.17, we have

$$log[c(x,y)] = log[\frac{1}{2} b(x,y)] + i\phi(x,y), \tag{2.19}$$

where the real and imaginary parts give, respectively, the logarithmic amplitude and phase of the independently separated fringe signal.Another approach to obtain the phase from $b(x,y)$ is to apply the function:

$$\phi(x,y) = tan^{-1}\frac{Im\left[c(x,y)\right]}{Re\left[c(x,y)\right]}. \tag{2.20}$$

The phase obtained from the imaginary part of Equation 2.20 is wrapped into the principal value $[-\pi,\pi]$, therefore, a phase unwrapping algorithm is necessary to recover the desired phase map [69].

2.5.3 Regularized phase tracking (RPT)

RPT is a phase and frequency tracking system capable of demodulating noisy broadband interferograms bounded by arbitrarily shaped pupils without introducing edge distortion. Proposed by Servin in [15], it is considered to be a nonlinear technique that allows phase demodulation of single-image closed-fringes interferogram. Another advantage of this method is that the phase obtained by the RPT system is continuous which does not require an unwrapping process. This is the first robust method capable of demodulating the phase of the closed fringe pattern in a fully automatic way.

Method

One of the main problems when dealing with this type of technique is, that there is no single solution due to the parity of the cosine function involved in the interference pattern. For this it is subjected to a regularization process to find an appropriate cost function that uses at least two terms that contribute to constraining the estimated phase field in a smooth way. These terms are related with the following information:

1. Fidelity between the estimated function and the observation.

2. Smoothness of the modulated phase field.

Specifically, in the RPT technique it is assumed that its irradiance may be modeled as a cosinusoidal function phase modulated by a plane. The amplitude of this cosinusoidal function must be close to the observed irradiance, and the second term of the proposed cost function refers to the expected smoothness and continuity of the estimated phase. In details, the proposed cost function to be minimized by the estimated phase $\phi_0(x,y)$ is:

$$U_T = \sum_{(x,y)\in L} U_{x,y}(\phi_0, \omega_x, \omega_y), \tag{2.21}$$

where

$$\begin{aligned} U_{x,y}(\phi_0, \omega_x, \omega_y) = \sum_{(\varepsilon,\eta)\in(N_{x,y}\cap L)} & (\{I'(\varepsilon,\eta) - cos[\phi_e(x,y,\varepsilon,\eta)]\}^2 \\ & +\lambda[\phi_0(\varepsilon,\eta) - \phi_e(x,y,\varepsilon,\eta)]^2 m(\varepsilon,\eta)), \end{aligned} \tag{2.22}$$

and

$$\phi_e(x,y,\varepsilon,\eta) = \phi_0(x,y) + \omega_x(x,y)(x-\varepsilon) + \omega_y(x,y)(y-\eta), \tag{2.23}$$

where L is a two-dimensional network that has the information of the fringes, $N_{x,y}$ is the neighborhood associated with the point (x,y), $m(x,y)$ is a field indicator that equals to 1 if at location (x,y) the phase has been calculated and 0 otherwise, ω_x and ω_y represent the local frequencies calculated along the x and y directions, respectively. The fringe pattern $I'(\varepsilon,\eta)$ is a high-pass filtered version of intensity pattern (Equation 2.1). This operation is done in order to eliminate the low-frequency background $a(x,y)$. Finally, λ is the regularizing parameter that controls the smoothness of the detected phase.

The first term of Equation 2.22 attempts to determine the fidelity between the found and observed fringe, the second term controls the level of smoothness and continuity of the fringe when demodulated in the least squares sense. To demodulate a fringe pattern it is necessary to find the minimum of the cost function $U(x,y)$ with respect to the fields $\phi_0(x,y)$, ω_x and ω_y, for this it is necessary to use the algorithm described in [15].

The results described by Servin demonstrate the demodulation capability of a single fringe pattern that has either closed or open fringes and can detect the modulating phase of noisy closed-fringe patterns in a fully automatic manner.

Chapter 3

Metaheuristics

3.1 Introduction

Metaheuristic procedures [70] were introduced in 1986 by Glover and this term derive from the composition of two Greek words heuristic which means *"to find"*, and meta, which means *"beyond, on a higher level"*. For this reason, metaheuristics are defined as intelligent algorithms to design or improve general heuristic procedures [71], that is, they are a class of approximation methods that are designed to solve difficult combinatorial optimization problems, as well as providing a general framework to create new hybrid algorithms combining different concepts derived from artificial intelligence, biological evolution and statistical methods.

Most combinatorial optimization problems are in practice generally difficult to solve. These problems are included in the class of NP-hard problems [72],since there are no exact algorithms with polynomial complexity known to solve them. Due to their intractability, a large number of approximate methods have been designed, which find good solutions in reasonable computational times. In this class of problems, the search for a solution requires an organized exploration through the search space: a search without a guide is extremely inefficient.

Many engineering problems can be formulated as optimization problems over an objective function defined over a domain $\mathbb{R}^n$ of attainable solutions. Solving them involves finding, within a defined domain, the solution that minimizes the objective function (global optimum).

This problem arises in many research and engineering problems, when it is necessary to obtain, from a set of solutions, the best one for a given problem, and a criterion capable of measuring the quality of each solution is available.
From a mathematical point of view, an optimization problem can be formulated as a term $(f, \chi, \mathbb{R}^n)$, where f is the function to be optimized; χ is the set of feasible solutions, and $\mathbb{R}^n$ is the solution space, i.e. the goal is to find a global optimum x^* such that:

$$x^* = argmin_{x \in \mathbb{R}^n} f(x), \tag{3.1}$$

with

$$x^* = (x_0, x_1, \ldots, x_n)^T \tag{3.2}$$

subject to a set of constraints that make up the feasible region χ.
Optimization models can be classified into 3 main groups:

- ✓ ***exact methods*** that are characterized by obtaining the optimal solution but are computationally slow.
- ✓ ***heuristics*** are those methods that are based on specific information of the problem and obtain sub-optimal solutions.
- ✓ ***metaheuristics*** establish general frameworks valid for any optimization problem obtaining approximate solutions (Figure 3.1).

In the development of metaheuristic procedures, it is important to take into consideration the definition of the operators that are in charge of directing the search to promising areas of the solution space. For this, two important factors must be taken into account [73]:

- ✓ ***Exploration***, also called diversification in the literature, is the process of guiding the search towards unexplored regions. An algorithm that performs insufficient exploration could miss entire regions, so if the optimum were found in one of those regions, it would have no chance of being found.

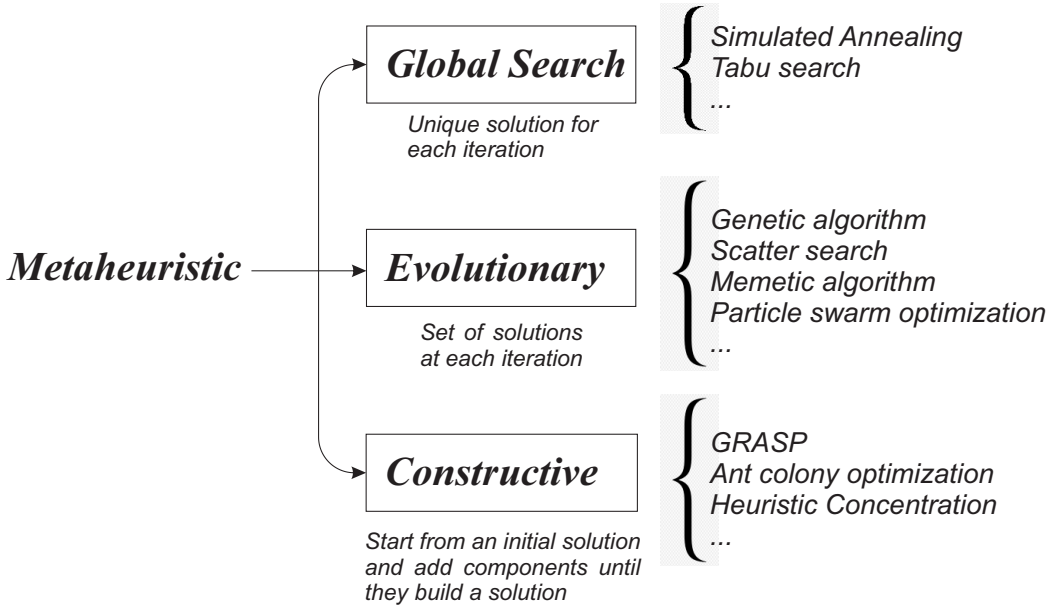

Fig. 3.1 Metaheuristics classification.

✓ ***Exploitation***, also called intensification in the literature, is the process of conducting a thorough and intense search for better solutions in an environment close to good solutions already found (considering that they are more promising areas). This process is essential to obtain greater precision in the solutions found.

In the specific case of metaheuristics, they are considered as a strategy that guides different subordinate heuristics to exploit and explore the solution space, so they are considered as intelligent strategies with high performance that do not guarantee optimality, but can yield feasible solutions in a reasonable time. This chapter provides a detailed description of the main metaheuristics used to address the problem proposed in Chapter 1.

3.2 Simulated annealing

The SA algorithm is considered within the category of local search, because they work with an initial solution, which is transformed into other better solutions as the search progresses. This is achieved by small perturbations in the current solution. If the changes improve the current solution, it is replaced by the new solution found. This process continues until no better

solution can be found or a stopping criterion is met. The solution found is not necessarily the global optimum. This type of basic local search algorithm has the disadvantage that it is susceptible to being easily trapped in local optima.

To avoid this problem, some moves are usually allowed to produce configurations that make the current solution worse. Such moves help to escape local optima, but they must be performed in a controlled manner. In RS this is done in a probabilistic manner due to its stochastic search approach.

This technique was formulated by Kirkpatrick et al. in 1983 [74], and has since proven its efficiency in solving a number of optimization problems applied to science and engineering. Its name is based on an algorithm developed in 1953 [75], where a Monte Carlo method was implemented to calculate the properties of any material or substance composed of individually interacting molecules.

SA has great impact in the field of metaheuristics due to its simplicity and efficiency in solving combinatorial optimization problems. It is inspired by the annealing process of metals, in which it is required to subject them to high temperatures and then slowly cool them. The cooling process has a great impact on the strength of the metal. If the cooling rate is slow, a strong metal will be obtained. On the other hand, if the initial initial temperature is not sufficiently high, a state called metastable is reached, in which the metal has imperfections and lacks strength [13].

3.2.1 Basic description

The SA algorithm starts from a solution, and a high initial temperature. From this level the temperature is slowly lowered, at each level a number N of solutions is explored in a predefined neighborhood, which are accepted if they outperform the starting solution in fitness. Otherwise, they are admitted as new solutions with a certain probability:

$$p(\Delta f, T) = e^{-\frac{\Delta f}{T}}, \tag{3.3}$$

where $\Delta f = f_{Candidate} - f_{Current}$ and represents the increment of the fitness function, while T indicates the temperature level. This function is known as the Metropolis acceptance criterion [75].

The probability p of accepting a solution far from the optimum solution is directly proportional to the temperature; this variant causes RS to avoid stagnation in local optima. The above process is repeated until a stopping condition is satisfied. The pseudocode of the RS algorithm is shown in Algorithm 1.

Algorithm 1 Simulated Annealing

procedure SIMULATED ANNEALING
    $f(S) \rightarrow$ *Fitness function*
    $N(S)) \rightarrow$ *Neighborhood*
    $S_0 \rightarrow$ *Initial Solution*
    $T_0 \rightarrow$ *Initial temperature*
    $\alpha \rightarrow$ *Temperature Function*
    $nrep \rightarrow$ *Iterations per level of temperature*
    $STOP \rightarrow$ *Stopping Condition*
    while STOP Conditions **do**
        Generate a random solution $S \in N(S)$
        $\Delta f = f(S) - f(S_0)$
        for $i : nrep$ **do**
            if $\Delta f \leq 0$ **then**
                $S_0 \leftarrow S$
            else
                Randomly generated $u \in U(0,1)$
                if $u \leq e^{-\frac{\Delta f}{T}}$ **then**
                $S_0 \leftarrow S$
                end if
            end if
        end for
        $T = \alpha(T)$
    end while
    Return the best solution
end procedure

3.3 Variable mesh optimization

Variable mesh optimization (VMO) is a population-based metaheuristic with evolutionary characteristics where a set of nodes representing potential solutions to an optimization problem form a mesh (population) that dynamically grows and moves through the search space (evolves) [76]. For this, an expansion process is performed in each cycle, where new nodes are generated in the direction of the local extremes (nodes of the mesh with better quality in different neighborhoods) and the global extreme (node obtained with better quality in the whole process developed); as well as from the border nodes of the mesh. Then, a mesh contraction process is performed, where the best representatives of each exploited zone of the search space are selected as the initial mesh for the next iteration. The general formulation of the meta heuristic covers both continuous and discrete optimization problems, in our case we will emphasize continuous problems.

3.3.1 Metaheuristic overview

The essence of the VMO method is to create a mesh of points in the m dimensional space, where the optimization process of a function $F(x_1, x_2, \ldots, x_m)$ is performed; which is moved by a process of expansion towards other regions of the search space. This mesh becomes "finer" in those areas that seem to be more promising. It is variable in the sense that the mesh changes its size (number of nodes) and configuration during the search process. The nodes are represented as vectors of the form $n(x_1, x_2, \ldots, x_m)$.
The node generation process in each cycle comprises the following steps:

- ✓ Initial mesh generation.
- ✓ Generation of nodes in the direction of the local extremes (nl).
- ✓ Generation of nodes in the direction of the global extremes (ng).
- ✓ Node generation from mesh boundaries (nf).

The method includes the following parameters:

- ✓ Number of nodes of the initial mesh (P).
- ✓ Maximum number of new nodes required in the expansion process (T) , where $3P \leq T$.
- ✓ Size of the neighborhood (k).
- ✓ Stopping condition (C) maximum number of fitness evaluations.

A more detailed description of each of the VMO steps in the process of generating new nodes (expansion) is presented below:

Initial mesh generation

The initial mesh consists of P nodes, which in the first iteration are generated randomly or by another method that guarantees to obtain different solutions.

Nodes generation towards local extremes in the neighborhood

The first type of exploration performed in VMO is carried out in the neighborhoods of each of the nodes of the initial mesh. This step is responsible for performing an intensification of the search in the neighborhood of each node to calculate the nearest neighbors of each node of the mesh using the Euclidean distance as the distance function, defined by:

$$D_{euclidean}(n_1, n_2) = \sqrt{\sum_{i=1}^{M} (n_1(i) - n_2(i))^2} \, . \tag{3.4}$$

The proximity of the new node to the current or local end depends on a factor (Pr), calculated on the basis of the values reached by the F at each of the nodes involved.
The greater the difference between the F values in the involved nodes, the greater the closeness or similarity of n to nl; this is guaranteed by the Pr factor, calculated using the following equation:

$$Pr(n, nl) = \frac{1}{1 + |Fitness(n) - Fitness(nl)|} \, . \tag{3.5}$$

This way of calculating Pr can be used to minimize as well as to maximize an objective function, since it only measures the separability ratio between two values, the case of study is not of interest.

Then the component values of the new node are calculated using the equation:

$$n*(i) = F(n(i), nl(i), Pr), \tag{3.6}$$

where the function F for the generation of new nodes from each node of the initial mesh, other than local extremes, and best neighbors, is defined by the equation:

$$n^*(i) = \begin{cases} \overline{m_i}, & \text{if } |\overline{m_i} - ne(i)| > \xi \quad \& \quad U[0,1] \leq Pr(n_i, n_i^*), \\ ne(i) + U[-\xi, \xi], & \text{if } |\overline{m_i} - ne(i)| > \xi, \\ U[\overline{m_i}, ne(i)], & \text{other case.} \end{cases} \tag{3.7}$$

where $\overline{m_i}$ represents the mean value between the current node (n), and the local end (ne) for the ith dimension and is calculated as:

$$\overline{m_i} = \frac{n(i) + ne(i)}{2}. \tag{3.8}$$

Furthermore, $U[a,b]$ represent a random value in the interval $[a,b]$, and ξ is an adaptive distance coordinate and is calculated according to Equation 3.8:

$$\xi_j = \begin{cases} \frac{range(a_i,b_i)}{4} & \text{if} \quad j < 15\%C \\ \frac{range(a_i,b_i)}{8} & \text{if} \quad 15\%C \leq j < 30\%C \\ \frac{range(a_i,b_i)}{16} & \text{if} \quad 30\%C \leq j < 60\%C \\ \frac{range(a_i,b_i)}{50} & \text{if} \quad 60\%C \leq j < 80\%C \\ \frac{range(a_i,b_i)}{100} & \text{if} \quad j \geq 80\%C \end{cases}, \tag{3.9}$$

where C denotes the maximum value of evaluations of the objective function, j the current evaluation, $range(a_i,b_i)$ denotes the domain amplitude (a_i,b_i) of each component. On the

other hand, depending on the percent of the total represented by the current evaluation, distance values representing parts of the allowed interval are defined.

Node generation in the direction of the global extreme

In this step of the generation, new nodes are created from each node of the initial mesh in the direction of the global extreme (ng) with the objective of accelerating the convergence algorithm. The new node (n_g^*) is generated using Equation 3.10:

$$n_g^* = G(n(i), ng(i), Pr(n, ng)), \tag{3.10}$$

In Equation 3.11 we present the G function used in this work, where $n_g^*(i)$ represents the values computed for each component of the new nodes n_g^*.

$$n_g^*(i) = \begin{cases} average(n(i), ng(i)) & \text{if} \quad U[0,1] \leq Pr(n, ng) \\ U[average(n(i), ng(i)), ng(i)], & \text{otherwise.} \end{cases} \tag{3.11}$$

Nodes generation starting from the frontier nodes of mesh

In this step, the total number of nodes that the mesh should have is completed, starting from the border nodes. To detect this type of nodes we use, for this case study, the value of the norm of each one, defined by

$$\|n\| = \sqrt{\sum_{i=1}^{m} n(i)^2}. \tag{3.12}$$

The higher norm nodes are those located on the contour of the initial mesh (n_s), and those of a lower norm are considered to be the nodes closest to the origin (n_u). Starting from these sets, new nodes are created (one for each frontier node) using the function H (see Equation 3.13).

$$nf = H(n_{s|u}, w). \tag{3.13}$$

The function H allows to generate new nodes in the direction of the boundaries defined for this case study, by means of the expressions:
For the outermost nodes:

$$n_s(i)^* = \begin{cases} n_s(i) + U[-1,1]w. \end{cases} \tag{3.14}$$

For the innermost nodes:

$$n_u(i)^* = \begin{cases} n_u(i) + U[-1,1]w, \end{cases} \tag{3.15}$$

where the displacement w_i is calculated as:

$$w_i = (w_i^0 - w_i^1)\frac{C-c}{C} + w_i^1, \tag{3.16}$$

where the parameter C, and the variable c, are closely related and cause the variations in the value of w_i; the first represents the total number of evaluations of the objective function, and the second denotes the number of the current evaluation. In turn, w_j represents a displacement for each component ith, where the variables w_j^0 and w_j^1 represents the initial and final displacement value. In order to obtain decreasing displacements $w_j^0 > w_j^1$ and its values are calculated as: $w_j^0 = \frac{range(a_i,b_i)}{10}$ and $w_j^1 = \frac{range(a_i,b_i)}{100}$.

Mesh contraction process

The contraction operation selects those individuals that will be used for the next algorithm iteration. Thus, based on an elitist strategy, nodes are sorted by their fitness values in such a way that survivor selection begins for that node with the best fitness. Before selection, a clearing operator is applied to keep a minimum distance between the mesh node. This mechanism considers two important elements, the node qualities and their places in the solution space, and increases the method's exploitation level and makes it stronger.

Chapter 4

Parallel methods applied to fringe pattern demodulating

4.1 Introduction

During the last years, several fringe analysis algorithms that using soft computing like neural networks and optimization models have been proposed. Among the main approaches that use the neural network technique is the works presented by Cuevas et al. [77, 78], where a multi-layer neural network is trained by using fringe patterns and the phase gradients associated with them, from calibrated objects. Methods using an optimization model approximate the phase through the estimation of parametric functions, for example soft computing techniques applied to Zernike polynomials [45], combination of Genetic Algorithms and parametric methods[38, 42, 46], Particle Swarm Optimization [79], and Harmony Search Optimization [48], among others.

In the present chapter, a method is proposed to obtain a parametric approach, using the Simulated Annealing (SA) technique, to determine the phase term $\phi(x,y)$ from a single fringe pattern using parallel computing. This method represents a modification of the Fringe Processing on Independent Windows (FPIW) proposed by Toledo and Cuevas [46] to demodulate complicated fringe patterns using SA to fit a polynomial on sub-sampled images.

Another important aspect to be discussed in this chapter is the introduction of a new model

for the demodulation of fringe patterns using an optimization algorithm. This model has the particularity that it implements the new population metaheuristic called "Variable Mesh Optimization" (VMO) [76], and introduces a novel methodology using Bernstein polynomials to fit the phase and estimate the points control of the mesh generated by the Bezier surface using a global optimization algorithm.

4.2 Parallel Demodulation Algorithm

In the proposed method, a fringe pattern is partitioned into independent windows that contain a number of fringes less than or equal to a value provided as a parameter. Then, a polynomial function is fitted to approximate the phase field of each window using SA algorithm as a global optimization method. This procedure is applied in parallel over all sub-images partitioned. At the end, a splicing procedure is required to connect different SA fitted phase windows and determine the whole phase field $\phi(x,y)$. The complete parallel demodulation process is overriding in the next subsection.

4.2.1 Algorithm for automatic partition of an interferogram (API)

The first part of this work is based on implementing an algorithm which can autonomously divide an fringe pattern into the maximum number of fringes desired in each window. This process consists of obtaining the lowest amount of subimages consistent with the number of allowed fringes. For this purpose, a tree-type data structure was implemented [80], where each leaf of the tree represents a partition of the fringe pattern. Figure 4.1 shows the general scheme of the employed data structure.

API is a recursive method that implements a post-order traversal and verifies that each sheet complies with the number of fringes restriction. The algorithm verifies if the node has a child, and if so, the recursive method with all the children is called again. Otherwise, the node is a leaf, and it is verified whether it complies with the number of fringes restriction. If it does, the process for that window is stopped; otherwise, the interferogram is partitioned into 4

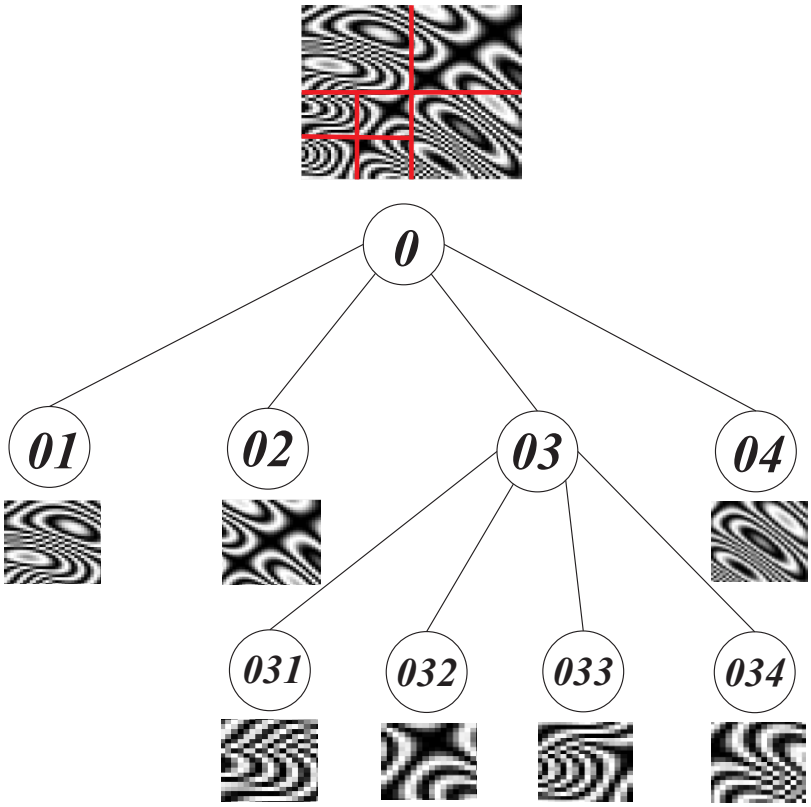

Fig. 4.1 Diagram of the data structure used to store the windows of the interferograms divided by the algorithm.(Image was taken from [1])

subimages. The process is repeated until all sheets have the maximum number of required fringes. Algorithm 2 shows the pseudo-code for API.

4.2.2 Parallel analysis of fringe patterns using a SA algorithm

The analysis of fringe patterns mainly focuses on the precision, automaticity, and speed. There are two ways to accelerate the speed of an algorithm, the first one is decreasing the computational complexity of the algorithm, and the second by hardware.

The presented technique aims to address the concept of parallel computing and its applications in the analysis of fringe patterns by modeling the problem in such a way that it can be divided into n independent tasks. In this work a fringe pattern is partitioned into independent windows, which are fitted to approximate the phase field of each subimage by means of a parametric function. A SA is used to find the functions parameters by the optimization of an Objective

Algorithm 2 API Algorithm

```
1: procedure WINPARTITIONR
2:     Input:
3:     Node → Fringe pattern
4:     N → Fringes Number
5:     Tree → Data Structure
6:     if Node != null then
7:         FirstSon = Node.getFirst_Son
8:         while FirstSon != null do
9:             FirstSon = FirstSon.getFollow_Brother
10:            WinPartitionR(FirstSon, N, Tree)
11:        end while
12:        if Node.getFirst_Son == null then
13:            if Node.getFringes > N then
14:                arraySons = Partition(Nodo)
15:                Tree.add(arraySons)
16:            end if
17:        end if
18:    end if
19:    Output: Tree
20: end procedure
```

Function (F) [38]. The fitness function is composed of two terms: the first term refers to the fringe similarity criterion, and the second indicates the smoothness criterion where the sum of the cross-gradients that yield soft solutions is penalized. When the information about the shape of the object $\phi(x,y)$ is unknown, a polynomial adjustment is recommended. An F for each sub-image is used to obtain the fitness value; it can be written as:

$$\begin{aligned} F &= \sum_{y=1}^{R}\sum_{x=1}^{C}\Big\{ \big(I(x,y) - (128 - 127\cos[\phi(x,y)]) \big)^2 \\ &+ \mu\big[\big(\phi(x,y) - \phi(x+1,y+1)\big)^2 + \big(\phi(x+1,y) - \phi(x,y+1)\big)^2\big] \Big\}, \end{aligned} \tag{4.1}$$

where x and y are integer values that indicate the position of the pixels in the fringe pattern, μ is the smoothness factor, which penalizes high sums of gradients to provoke smooth solutions, $I(x,y)$ is the intensity value detected at the point (x,y) and $\phi(x,y)$ represents the two-dimensional polynomial approximation of degree n, which during the optimization

process given by:

$$\phi(x,y) = s_0 + s_1x + s_2y + s_3xy + s_4x^2 + s_5y^2 + \cdots + s_{\frac{(n+1)(n+2)}{2}-1}y^n, \tag{4.2}$$

where the terms s_i represent the coefficients of the polynomial that approximate the phase term.

4.2.3 Initial solution

For this study, random generation of the initial solution S is used, which is a vector of n-parameters, where each s_i term indicates a coefficient of a possible approximation, from Equation 4.4:

$$S = \left[s_0, s_1, s_2, \ldots, s_{\frac{(n+1)(n+2)}{2}}\right], \tag{4.3}$$

where each s_i term is a real value within a range defined by the user $[Inf_i, Sup_i]$. These values can be taken from prior knowledge, if it is available.

To define the search interval it is necessary to involve the a priori knowledge of the problem in question. It is known that the equation that models an interference pattern has a cosine profile which indicates that between each maximum or minimum of the cosine function there are 2π radians, this means, in each interval of 2π radians there is one white and one black fringe. This implies that each term s_i contributes to the total of radians within the fringe pattern which is related by:

$$\max(\phi(x,y)) - \min(\phi(x,y)) = 2\pi F, \tag{4.4}$$

where F represents the number of interferogram fringes.

Assuming the maximum values of the variables x and y, and making an iterative process where one coefficient is taken and the rest of the coefficients are made zero, it can find the

interval of each coefficient from the following mathematical statements:

$$\begin{aligned}
s_0 &= 2\pi F \ \rightarrow s_0 \in [-2\pi F, 2\pi F], \\
s_1 &= \frac{2\pi F}{X_{max}} \ \rightarrow s_1 \in \left[-\frac{2\pi F}{X_{max}}, \frac{2\pi F}{X_{max}}\right], \\
s_2 &= \frac{2\pi F}{Y_{max}} \ \rightarrow s_2 \in \left[-\frac{2\pi F}{Y_{max}}, \frac{2\pi F}{Y_{max}}\right], \\
&\vdots \qquad\qquad\qquad\qquad \vdots \\
s_{\frac{(n+1)(n+2)}{2}-1} &= \frac{2\pi F}{(Y_{max})^n} \ \rightarrow s_n \in \left[-\frac{2\pi F}{(Y_{max})^n}, \frac{2\pi F}{(Y_{max})^n}\right],
\end{aligned} \tag{4.5}$$

where Y_{max} and X_{max} represent the number of rows and columns of the fringe pattern.

4.2.4 Neighborhood solution

One of the factors that influence the efficiency of the SA algorithm is the vicinity function used during the optimization process [81]. The objective of the vicinity function is to provide a solution s_{i+1} through an operator of movements, which slightly alters the solution s_i. For this purpose, it is necessary to establish how to get the solutions that make up the vicinity given a particular solution and how to select one of them as a candidate for a new solution. In this work, a greedy search is performed to generate N neighboring solutions. New local solutions are generated by varying each coefficient s_n of the initial solution, and thus obtaining a neighborhood from which the best element is selected. The current coefficients s_n are modified using the following equation:

$$s_i = s_i + U[\alpha_i * a_i, \ \alpha_i * b_i], \tag{4.6}$$

where $U[a,b]$ generates a random number with a uniform distribution in the range [a, b], a_i and b_i represent the upper and lower limits of the allowable space for each coefficient, respectively, and α is a parameter that depends on the Boltzmann temperature function, because its objective is to delimit the interval of each coefficient and just as the temperature

function, α decrements the interval in each iteration. In addition, if a coefficient exceeds the definition limits, it is penalized and a new random value is generated in the allowable space.

4.2.5 Cooling schedule and stop conditions

The cooling scheme in the SA must provide a good compromise between the execution time and the quality of the final solution. There are several studies focused on cooling programs, among which [82] and [83] are noteworthy. In this case, a function is defined which ensures that the temperature gradually decreases with the number of iterations ensuring that the temperature reaches its minimum value in the last iteration. The following equation shows the implemented temperature function:

$$T(i) = e^{-10^{-6}*i^2+\frac{log(\frac{10*T_f}{T_0})}{N}+N*10^{-6}+log(T_0)}, \tag{4.7}$$

where i represents the current iteration, N the number of iterations, T_0 and T_f indicate the initial and final temperatures of the model. For instance, having $N = 800,\ T_0 = 12000$ y $T_f = 1$, Equation 4.7 has the following behavior, shown in Figure 4.2. The temperature function is related to the number of iterations and the limits of desired temperature, the SA does not stop until both conditions are met.

Another cooling mechanism used in this project was that presented by Toledo and Cuevas in [46]. Basically, it consists of starting from a temperature value large enough for the system to reach its steady state for that temperature. In this way, there is the opportunity to explore all the space of solution, so the probability of falling in a local minimum is decreased. T is varied by:

$$T(i) = T_0\ exp(-i/k), \tag{4.8}$$

where k is a constant that indicate in which generation $T(i) \approx T_0/3$.

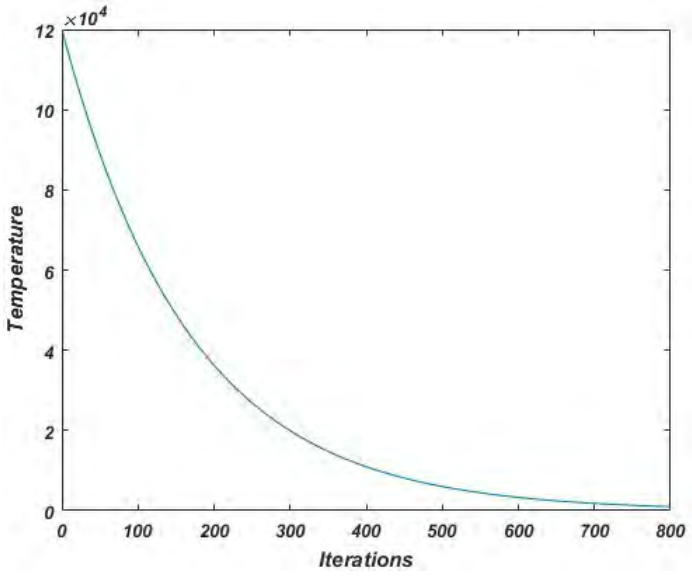

Fig. 4.2 Temperature function generated from Equation 4.7

4.2.6 Unification of the phase from the independent windows

The phase demodulation is achieved by window segmentation of the fringe pattern and is executed in separate tasks and in parallel. The splicing procedure used constitutes an improvement of the method presented by Toledo and Cuevas [46], because it avoids the use of overlapping regions in neighboring windows. Basically the phase windows linking method is composed of the following steps:

1. The phase of the first window adjusted by SA is taken as reference.

2. The neighboring phase $\phi(x,y)$ is selected and its phase is calculated with inverted concavity $\phi(x,y)^{'}$.

3. The modification consists in that the overlapping region that is chosen from the reference image, and it is done through polynomial approximation using cubic spline [84]. In other words, if the bordering region of the reference phase is the last row or column, or both, extrapolation is done to find the $n+1$ row or column corresponding to the current phase. Fig. 4.3 illustrate the procedure and a scheme of the extrapolation process.

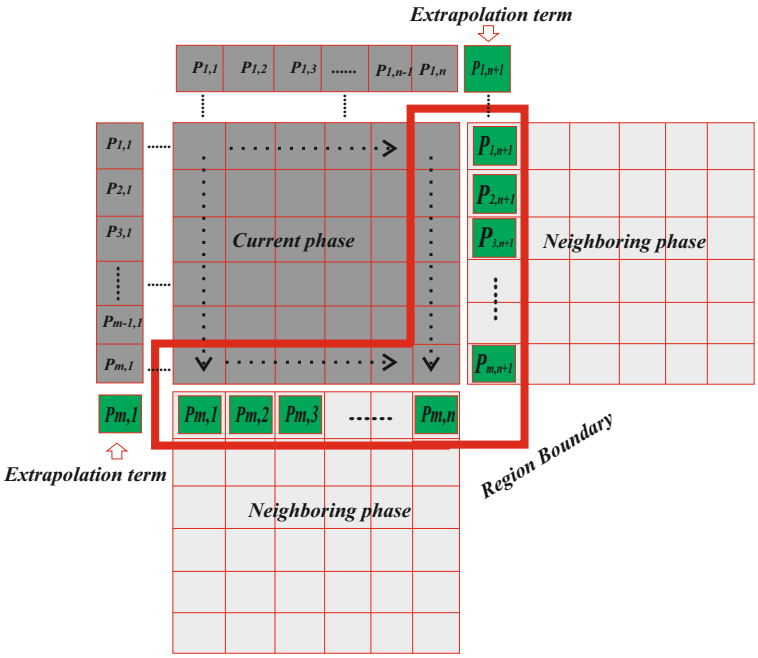

Fig. 4.3 Representation of the overlap region between neighboring windows. (Image have been taken from [1])

The DC or height difference between the frontier region for $\phi(x,y)$ and $\phi(x,y)'$ is calculated by the following expressions:

$$DC_1 = \frac{\sum_{x,y\in N}(\Theta(x,y) - \phi(x,y))}{A},$$
$$DC_2 = \frac{\sum_{x,y\in N}(\Theta(x,y) - \phi(x,y)')}{A}, \tag{4.9}$$

where $\Theta(x,y)$ is the region extrapolated by spline cubic, N is the border region, and A is the area $(pixel^2)$ of the region.

4. The mean squared error for both alternatives is calculated as follows, with the aim of making a comparison between both.

$$RMS_1 = \frac{\sum_{x,y\in N}(\Theta(x,y) - \phi(x,y) - DC_1)^2}{A},$$
$$RMS_2 = \frac{\sum_{x,y\in N}(\Theta(x,y) - \phi(x,y)' - DC_2)^2}{A}. \tag{4.10}$$

The phase with the lowest RMS will be displaced by a value of $\phi(x,y) + DC1$ or $\phi(x,y)' + DC2$ to place it at the level of the reference phase map.

5. The process is repeated until each phase map has been moved.

4.2.7 Surface smoothing

Low pass filtering (aka smoothing), is employed to remove high spatial frequency noise from a digital image. The low-pass filters usually employ moving window operator which affects one pixel of the image at a time, changing its value by some function of a local region (window) of pixels. The operator moves over the image to affect all the pixels in the image. For this work, these filters are used to smooth the phase surface, especially in those regions where neighboring windows are feathered. This process is performed at the end of the unification process of all independently demodulated windows.

4.3 Demodulation of fringe pattern using Bezier surface

This section presents a method to demodulate complex fringe images, based on the parallel demodulation algorithm [1]. Our model has the particularity that it implements the new population meta-heuristic called "Variable Mesh Optimization" (VMO) [76], and introduces a novel methodology using Bernstein polynomials to fit the phase and estimate the control points of the mesh generated by the Bezier surface using a global optimization algorithm.

4.3.1 Bernstein polynomials

In mathematics, the Bernstein polynomial is a polynomial that is a linear combination of Bernstein basis polynomials. The idea was introduced by Joseph Bernstein [85, 86] and Mikio Sato and Takuro Shintani [87]. Probably, polynomials in Bernstein form were first used by Bernstein in a constructive proof for the Weierstrass approximation theorem. With the advent of computer graphics, Bernstein polynomials, restricted to the interval $[0,1]$, became in one of the most practical uses of the Bernstein polynomials (Bézier curves and surfaces),

which can be used to approximate any curve or surface to a high degree of accuracy.
The Bernstein polynomials B_i^n of degree n form a basis for the vector space of polynomials of degree lower than or equal to n over the interval [0, 1] and are defined by:

$$B_i^n = \binom{n}{i} t^i (1-t)^{n-i} \quad i = 1, 2, \cdots, n, \tag{4.11}$$

where t is a variable, which can be generalized to cover an arbitrary interval $[a,b]$ by standardizing t over interval, $t = (x-a)/(b-a)$. Consequently, any polynomial curve $f(x)$ of a degree lower than or equal to n has a single representation of Bézier, which can be represented as a linear combination of the Bernstein polynomials of degree n,

$$f(x) = \sum_{i=0}^{n} B_i^n(x) P_j, \tag{4.12}$$

where P_j is a set of coefficients known as control points. Generalizing this concept over R^3 in the arbitrary interval $[a,b] \times [c,d]$, we can define Bezier's surface as the tensor product of Bernstein polynomials bases:

$$f(x,y) = \sum_{i=0}^{n} \sum_{j=0}^{m} B_i^n(x) B_j^m(y) P_{i,j}, \tag{4.13}$$

where $P_{i,j}$ is a control point matrix, and the surface is defined by $(n+1) \times (m+1)$ Bernstein polynomials bases. Thus, the resulting surface parameterization will be a bi-grade surface (m,n), and will be described by a control mesh (P_{ij}) of $(m+1) \times (n+1)$ vertices (see Figure 4.4).

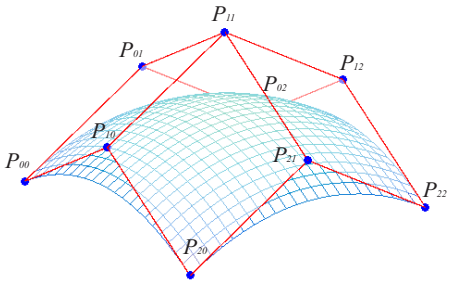

Fig. 4.4 Parametric representation of a Bezier surface.

4.3.2 Bezier surface properties

Bezier surfaces are a natural generalization of polynomial curves; that is why many of their properties remain [88]. Among the main useful properties in diverse applications are:

- The surface intuitively follows the general shape of the defining control mesh. This property is important for the posed problem, because sometimes, the shape of the object is known, and it is possible to generate an initial solution that defines a convex envelope of the object and facilitates the search process.

- The extreme vertices of the surface coincide with the corners of the control mesh, a property that leads to the rows and columns of the edge of the mesh describing the edge of the surface, i.e.

$$f(0,y) = \sum_{i=0}^{n}\sum_{j=0}^{m} B_i^n(0)B_j^m(y)P_{i,j} = \sum_{i=0}^{m} B_j^m(y)P_{0,j}. \tag{4.14}$$

- The surface is invariant when affine transforms are applied to either the control points or the parameterized surface.

- Local control is a property present on Bezier surfaces; therefore, a generic vertex of the control mesh affects most $(m+1)\times(n+1)$ sections of the surface. Obviously, a vertex near the edge affects fewer sections.

- The Bernstein polynomials of degree n can be defined by blending two Bernstein polynomials of degree $n-1$. That is, the ith nth-degree Bernstein polynomial can be written as:

$$B_i^n = (1-t)B_i^{n-1} + tB_{i-1}^{n-1}(t). \tag{4.15}$$

- The Bernstein Polynomials are all Non-Negative over the interval $[0,1]$. To show this we use the recursive definition property presented in 4.15, and mathematical induction. It is easily seen that the functions $B_0^1(t) = 1-t$ and $B_1^1(t) = t$ are both non-negative

for $0 \leq t \leq 1$. If we assume that all Bernstein polynomials of degree less than k are non-negative, then by using the recursive definition of the Bernstein polynomial, we can argue that $B_i^n(t)$ is also non-negative for $0 \leq t \leq 1$, since all components on the right-hand side of the equation are non-negative components for $0 \leq t \leq 1$. By induction, all Bernstein polynomials are non-negative for $0 \leq t \leq 1$.

4.3.3 VMO applied to demodulation interferogram

The present technique is based on the concept of parallel demodulation presented in the previous work [1]. A fringe pattern is subjected to a process of normalization with the aim of eliminating back lighting and modulating the signal amplitude; generically a low-pass filter is applied using the Fourier transform. After this, the resolution of the fringe pattern can be reduced to a resolution where the number of fringes in each window is maintained, thus speeding up the search system of the algorithm. Next, the fringe pattern is partitioned using the Algorithm for Automatic Partition of an Interferogram [1], which is used to divide an interferogram with a maximum limit of fringes in each window. Then, a demodulation method is applied simultaneously over each partition to approximate the phase field by means of the Bezier surface using VMO [89]. Finally, each corresponding real phase field is connected with different VMO fitted phase windows to determine the whole phase field $\phi(x,y)$ using the splicing procedure presented in [1].

4.3.3.1 Fringe pattern analysis using Bezier surface

Taking advantage of Bézier's surface properties, it is possible to obtain the edges of the control mesh by approximating the edges of the surfaces with the knowledge that the ends of the edges coincide with those of the surface, a property that facilitates the search process. This process is totally independent, and therefore, it is carried out in a parallel way. The next step is to eliminate the differences between the edges to form the outside of the control mesh. Finally, a search process is carried out from the limits of the control mesh. Figure 4.5 illustrates the scheme of the demodulation process using Bezier surfaces.

In this method, VMO is proposed to carry out the optimization process, where a parametric

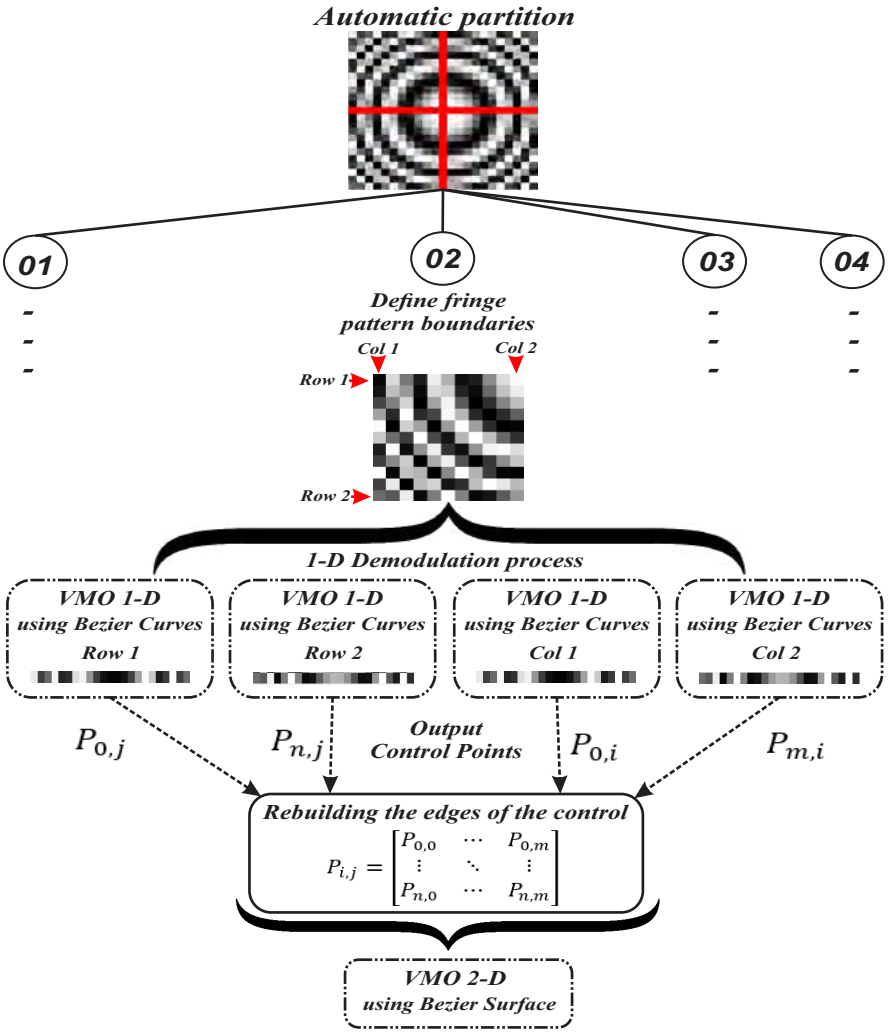

Fig. 4.5 Scheme of demodulation process using Bezier surfaces

estimation using Bezier surfaces is suggested to adjust the shape of the object involved in a fringe pattern. The fitness function, which is used to evaluate the quality of each node of the mesh, was proposed by Cuevas in [38] and it is shown in Equation 4.1. The only difference between the two functions is the fitting function that approximates the phase map; which was previously modeled by a polynomial fit and in this project we present a fit using Bézier surfaces. In conclusion, the demodulation process produces a phase map through a global optimization algorithm, where the main objective is to find a Bezier surface that generates a fringe pattern as similar as possible to the input interferogram.

4.3.4 Initial mesh generation and search interval

The initial population for the first iteration is composed of N nodes that are randomly generated with uniform distribution. This mesh is composed of N nodes $(s_1, s_2, \ldots, s_N)$, which represent potentials solutions in the search region. Each node is codified as a matrix $\mathbf{P}$ of $(n+1)\times(m+1)$ elements that defines the control mesh which generates the Bezier surface that fits the phase map of the fringe pattern, where n and m indicate the degree of the Bernstein polynomial on the x and y axes respectively,

$$\mathbf{P} = \begin{bmatrix} P_{00} & P_{01} & P_{02} & \ldots & P_{0n} \\ P_{10} & P_{11} & P_{12} & \ldots & P_{1n} \\ \vdots & \vdots & \vdots & \ddots & \vdots \\ P_{m0} & P_{m1} & P_{m2} & \ldots & P_{mn} \end{bmatrix}, \tag{4.16}$$

where each term $P_{i,j}$ is a real value within a defined range.

To define the search interval of each coefficient of the control matrix, it is necessary to use the a priori knowledge. Based on the property that the control mesh represents a convex envelope of the surface, and that the pattern of fringes has a cosine profile through which it is possible to know the phase difference from a fringe count, we can define each coefficient of the mesh in the interval $[-4\pi F,\ 4\pi F]$, where F represents the number of interferogram fringes.

Chapter 5

Experimental Results

5.1 Introduction

To validate the effectiveness of the proposed methods, an experimental analysis was carried out, involving synthetic fringe patterns. In these cases, an analysis is performed in terms of solution quality, convergence time and adjustment of the metaheuristic parameters. In addition, tests of real images obtained from an optical arrangement were included. All the experiments were tested in a standard node that has 24 cores (2 sockets Intel Xeon E5-2680 v3 at 2.5 GHz with 12 cores per socket) and 128 GB of shared RAM.

To define the quality of the solutions, Root Mean Squared (RMS) was selected as a metric, which is a frequently used measure of the differences between values (sample) predicted by a model or an estimator and the observed values. The RMS represents the square root of the second sample moment of the differences between predicted values and observed values or the quadratic mean of these differences. Equation 5.1 represents the error calculated for each approximation.

$$RMS = \sqrt{\frac{\sum_{y=1}^{R}\sum_{x=1}^{C}(f(x,y)-\phi(x,y))^2}{R*C}}, \tag{5.1}$$

where R and C correspond to the number of rows and columns of the fringe pattern, f and ϕ define the original phase map and the one recovered by the model, respectively.

Finally, a comparative study was carried out with computer simulated fringe patterns published in related works to prove the effectiveness of the method presented.

5.2 Parallel demodulation algorithm using Simulated Annealing

5.2.1 Stability and sensitivity analysis

The simulation 5.2.1 consisted of approximating a computer simulated pattern, where the mathematical model of the original phase map is given by:

$$\begin{aligned} f(x,y) &= (1.0052\times 10^{-3}(0.4x-40)(0.4y-50) \\ &+ 1.9284\times 10^{-4}(0.4x-40)(0.4y-50)^2) \\ &\times cos(\frac{-0.8x+0.00816y^2}{5})sin(\frac{-0.8y+.00336x^2}{7});\ x,y\in[-15,15], \end{aligned} \tag{5.2}$$

The objective of this experiment is to demonstrate the stability of the algorithm and to make a sensitivity study of parameters. The computer generated closed fringe pattern used as input of the algorithm has a resolution of 42×42 pixels.

The first step of the model is to apply the automatic partitioning, using as parameter a maximum number of fringes in each window equal to 3. The result of applying the API algorithm is shown in Figure 5.1.

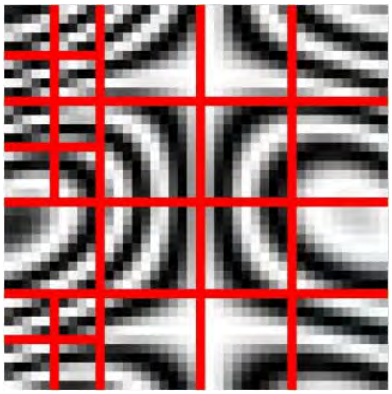

Fig. 5.1 Result of the automatic partition obtained by API.

Phase demodulation is achieved by segmenting the fringe pattern windows, using SA for each window independently, so this process is carried out in parallel. A total of 9 executions were made to perform a sensitivity analysis of the algorithm. Table 5.1 shows the configuration parameters used by SA and the results obtained in each execution.

Runs	Iterations	Generation per Iterations ($nrep$)	Initial Temperature	Smoot factor	RMS (radians)	Time (s)
1	300	50	900	5	0.0086	33
2	400	50	900	5	0.0061	44
3	500	50	900	5	0.0133	54
4	300	75	900	5	0.0060	49
5	400	75	900	5	0.0103	65
6	500	75	900	5	0.0065	82
7	300	100	900	5	0.0057	65
8	400	100	900	5	0.0051	87
9	500	100	900	5	0.0069	108
		Average			0.007611	65.2

Table 5.1 Results of 9 runs approximating the shape represented by Equation 5.2.

The resulting fringe pattern, related to the demodulated phase, and a comparison between both phase maps, corresponding to the execution number 8, are shown in Figure 5.2.

5.2.2 Sub-sampled fringe pattern

The computer generated fringe pattern 5.2.2 consisted of approximating a computer simulated interferogram, where the mathematical model of the original phase map is given by:

$$f(x,y) = (0.1x - 0.02y + 0.01xy - 0.02x^2)cos(\frac{x+y}{8}); \quad (5.3)$$
$$x \in [-32,-10] \text{ and } y \in [-15,20].$$

The objective of this experiment is to demonstrate the ability of the algorithm to recover phase in low resolution fringe patterns, even when the Nyquist criterion is not met. The

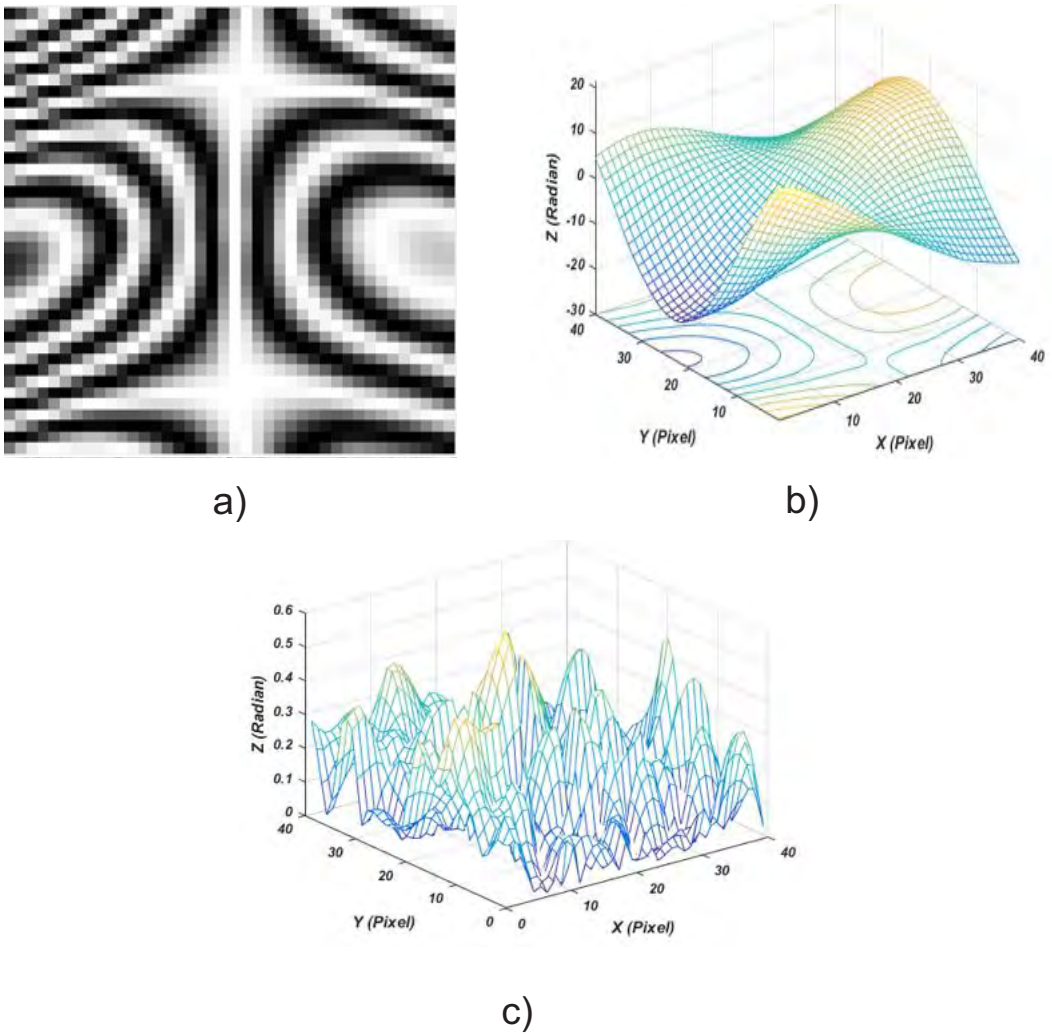

Fig. 5.2 a) Fringe pattern recovered by the method. b) Demodulated phase map. c) Error graph between original and demodulated phases.

computer simulation was reduced to a resolution of 36 × 36 pixels to be used as input to the algorithm and to apply an automatic partitioning with a maximum number of fringes equal to 5. The result of applying the API algorithm is shown in Figure 5.3.

Phase demodulation is achieved by segmenting the fringe pattern windows, using SA for each window independently, so this process is carried out in parallel. Each window was demodulated by adjusting a third degree polynomial during 200 iterations, with a generation of 50 neighboring solutions at each temperature level for a time of 109 seconds. The values of the initial temperature and the softness factor were 9000 and 15 respectively.

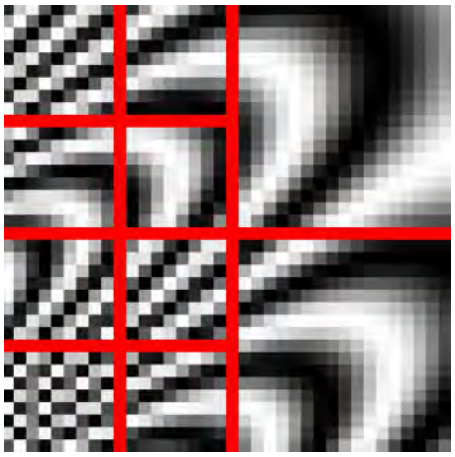

Fig. 5.3 Result of the automatic partition obtained by API in low resolution.

The resulting fringe pattern, related to the demodulated phase, and a comparison between both phase maps in high resolution, are shown in Figure 5.4. The root mean square (RMS) between the two phase maps was of 0.0073.

5.2.3 Computer simulated proposed by Toledo and Cuevas

The proposed method was tested to approximate the phase of a computer simulated fringe pattern suggested in [46]. The fringe pattern was sampled to produce an image of 54×54 pixels (Figure 5.5-a) and the result of applying the API algorithm, using a maximum number of fringes per window equal to 3, is shown in Figure 5.5-b.

A third degree polynomial was used to interpolate every partition. The values of the parameters used to achieve SA convergence were: generation number (N) of 300, starting temperature $T_0 = 11000$, the softness factor $\mu = 5$ and the number of neighboring solutions generated at each temperature level was 175.

The resulting fringe pattern and the map phase recovered by the method are shown in Figures 5.6-a and 5.6-b. For illustrative purposes, the difference between the computer simulated phase map and the one obtained during demodulation is shown in Figure 5.6-c. The root mean square (RMS) was used to measure the differences between simulated phase map and

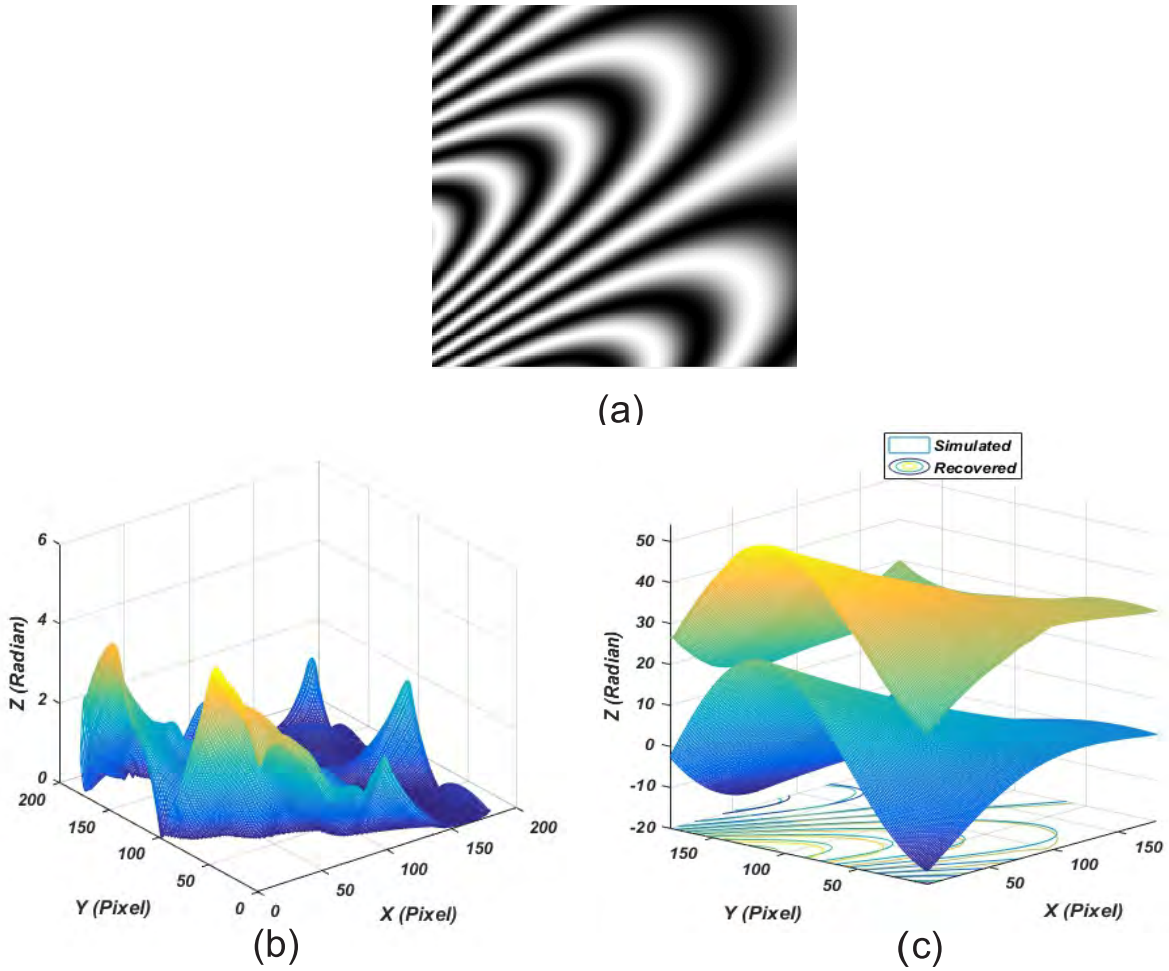

Fig. 5.4 a) Fringe pattern recovered by the method. b) Error graph between original and high resolution demodulated phases. c) High resolution demodulated and simulated phase map.

the one predicted by the model. The RMS error is 0.007 rad, this measurement is lower than the reported in [46] of 0.154 rad.

It is important to note that the main advantage of the proposed method over the traditional methods, is that in the recovery of fringe patterns that do not meet the Nyquist's criterion (i.e. when fringes are not fully sampled), this method is able to recover the phase term. When a comparative analysis with the model proposed by Toledo in [46] is carried out, the proposed method is able to obtain the phase map correctly reconstructed, in addition to introducing a new model of window partition, based on the frequency of the fringes per partition, which facilitates the use of the same configuration of SA parameters for each window. Another

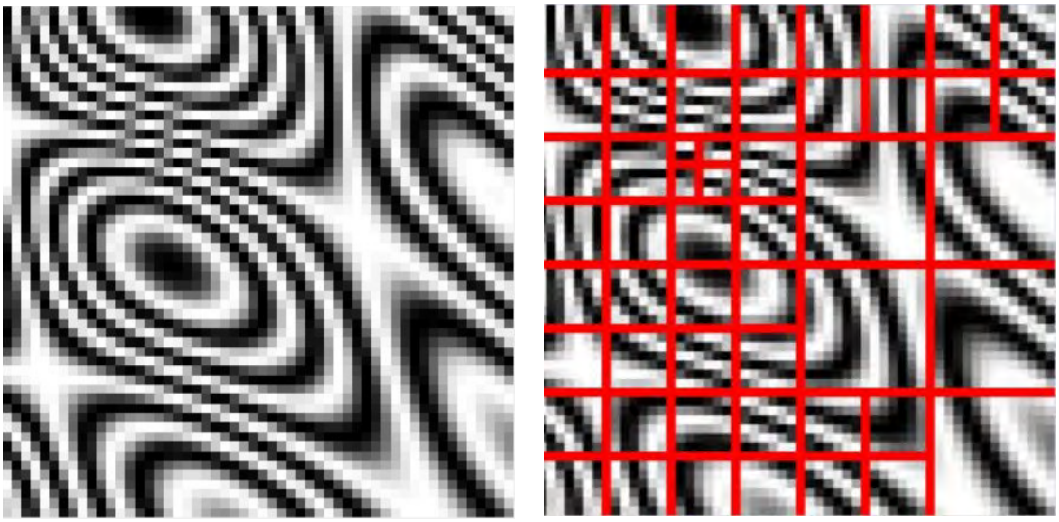

Fig. 5.5 (a) Sampled fringe pattern 54 $\times$ 54 pixel. (b) Result of the automatic partition obtained by API.

aspect to compare is that the proposed method does not use the concept of overlapped region between neighboring windows, offering as an advantage the fact that the same region is demodulated more than once. The last criterion that was compared was the speed, where the proposed model has a parallel implementation, as opposed to the serial implementation of [46], due to the fact that the process is divided into different independent tasks.

5.2.4 Semi-spherical surface obtained with shadow moire technique

This fringe pattern, taken into account in the experimental validation, corresponds to a fringe pattern obtained from a shadow moire experiment (Figure 5.7a). A hemi-spherical object was located behind a Ronchi ruling and was illuminated by a collimated beam. To reduce the search space of the algorithm, the resolution of the interferogram was reduced to 37x43 pixels and the image was binarized using the Otsu method [90] in small neighborhoods to ensure that background illumination and amplitude modulation were constant; and was later partitioned by the API algorithm, using a maximum number of fringes per window equal 4 (Figure 5.7b). The binarization process was performed in each window independently

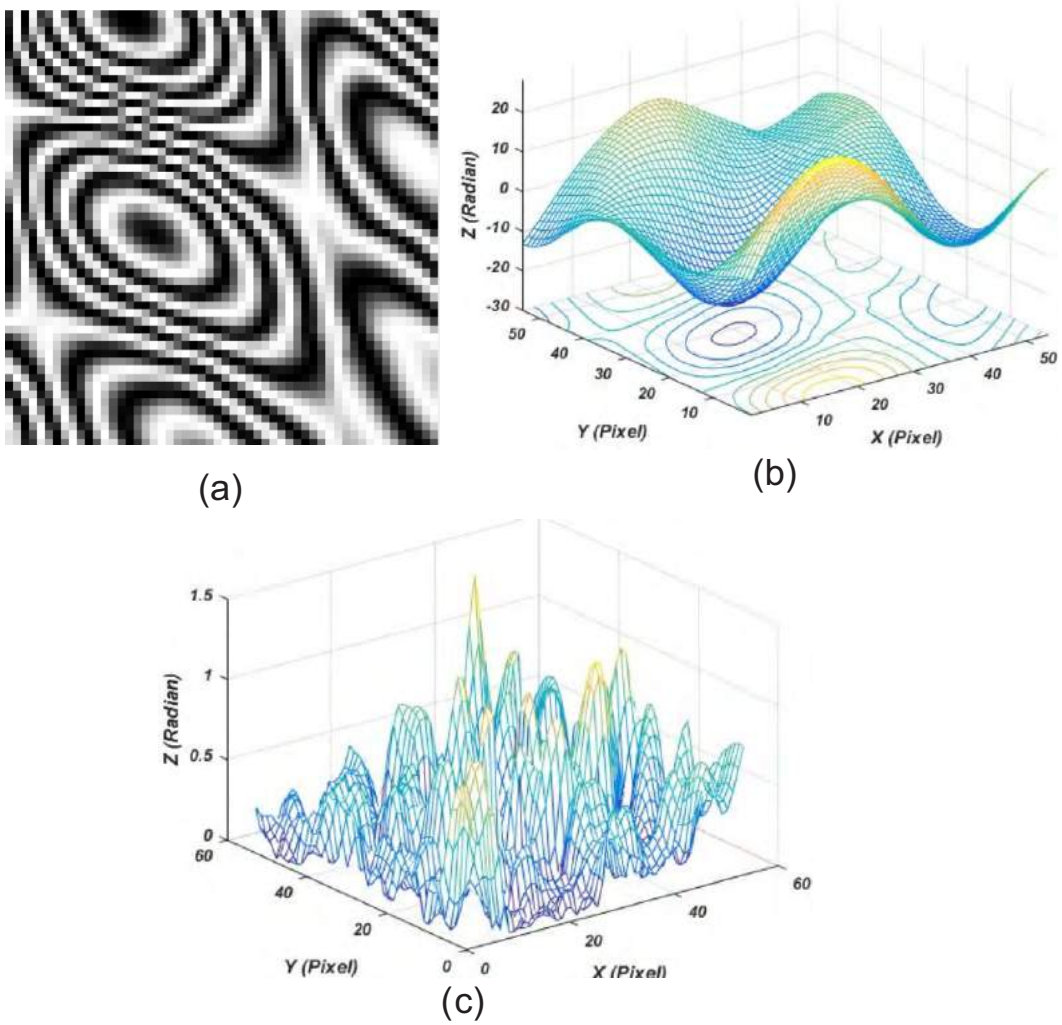

Fig. 5.6 (a) Fringe pattern recovered by the method. (b) Phase map demodulated. (c) Error graph between original and demodulated phase.

due to the different contrast variations in different positions, product of the lighting. The SA algorithm evolved during 3000 iterations to fit a second-degree polynomial to each sub-image in a period of 29 seconds. Thirty neighbors were generated in each iteration, the initial temperature used was 900, and the softness factor was 5. Figure 5.8 shows the results obtained by the demodulation process. It is worth noting that, a low-pass filter was applied to the phase map obtained after applying the unification algorithm of the windows to eliminate the roughness between the limits of the windows.

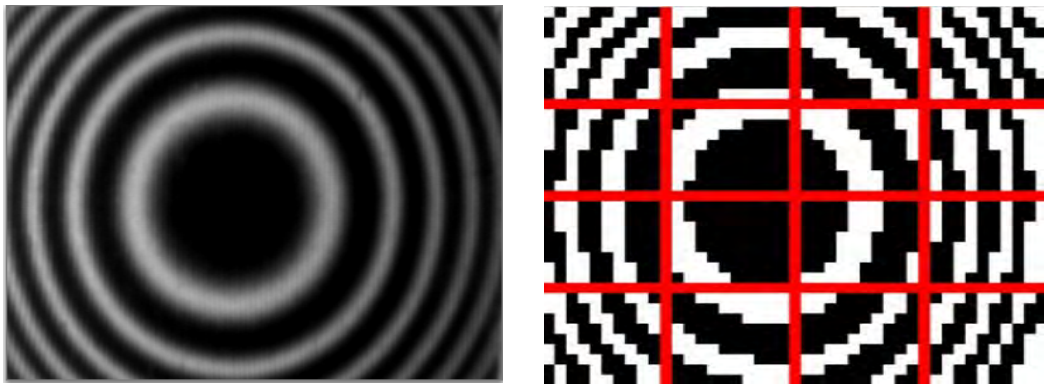

(a) (b)

Fig. 5.7 (a) The shadow fringe pattern generated by a hemi-spherical object with resolution of 244 $\times$ 281 pixels. (b) Independent windows partition carried out by IPA.

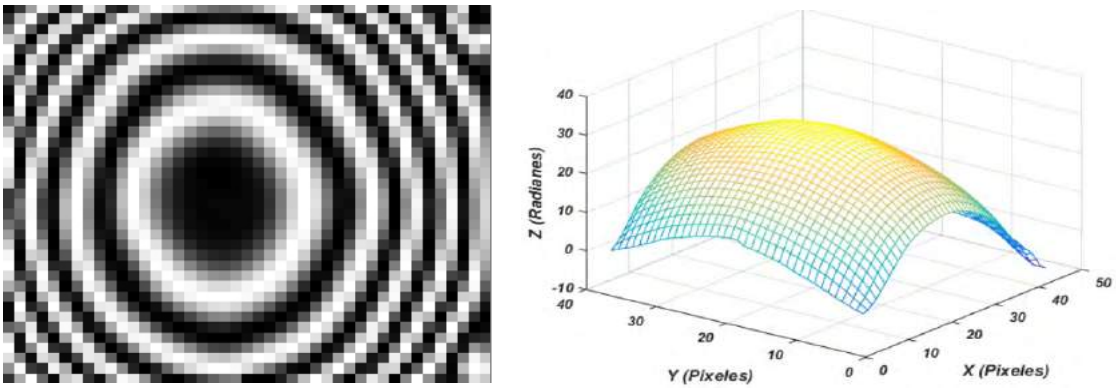

(a) (b)

Fig. 5.8 (a) Fringe pattern generated from the calculated phase field by the method. (b) Phase map recovered during the demodulation process.

5.2.5 Shadow moire experiment

The next fringe pattern used to test the model corresponds to a real shadow moire application (Figure 5.9 a), in which a low-pass filter is applied to eliminate the high frequencies produced by the grid. The original image was reduced to a resolution of 35 x 41 pixels and binarized using the Otsu method to serve as an input to the algorithm (Figure 5.9 b) , which was partitioned into windows with a maximum number of fringes equal to 4.

The SA algorithm needed 200 iterations and 50 neighbors in each loop to adjust a third-degree polynomial to each window, and it took 65 seconds to get the solution. The initial temperature

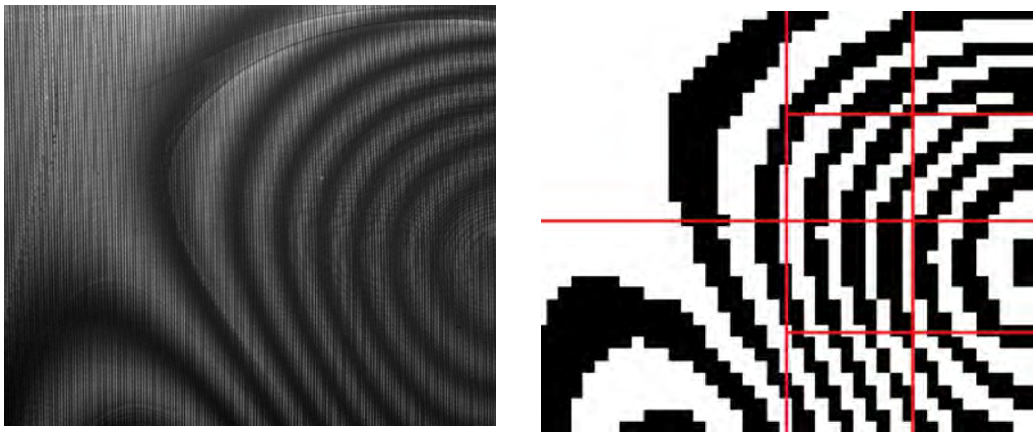

(a) (b)

Fig. 5.9 a) Original shadow Moire fringe pattern, with resolution of 831 $\times$ 971 pixel. b) Independent windows partition, carried out by IPA with resolution of 35 $\times$ 41 pixels.

and the softness factor had the same configuration as in the second interferogram to acquire the phase map. The resulting graph obtained by this method is shown in Figure 5.10.

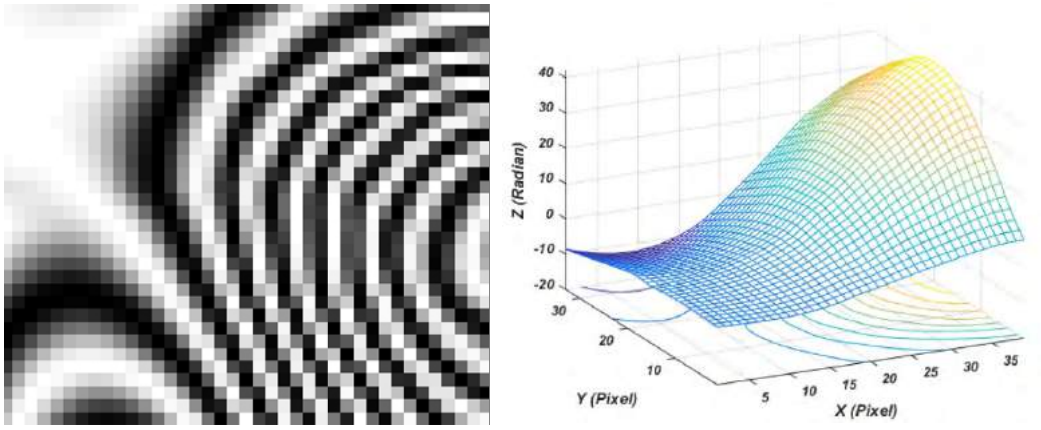

(a) (b)

Fig. 5.10 a) Fringe image obtained from the proposed method. b) Phase map recovered from the interferogram of Figure 5.9 b.

5.2.6 Speckle interferometry experiment

The fifth experiment corresponds to a real interferogram, which presented a greater amount of noise, since it was obtained from a speckle interferometry experiment. The results of applying the algorithm are shown in Figure 5.11.

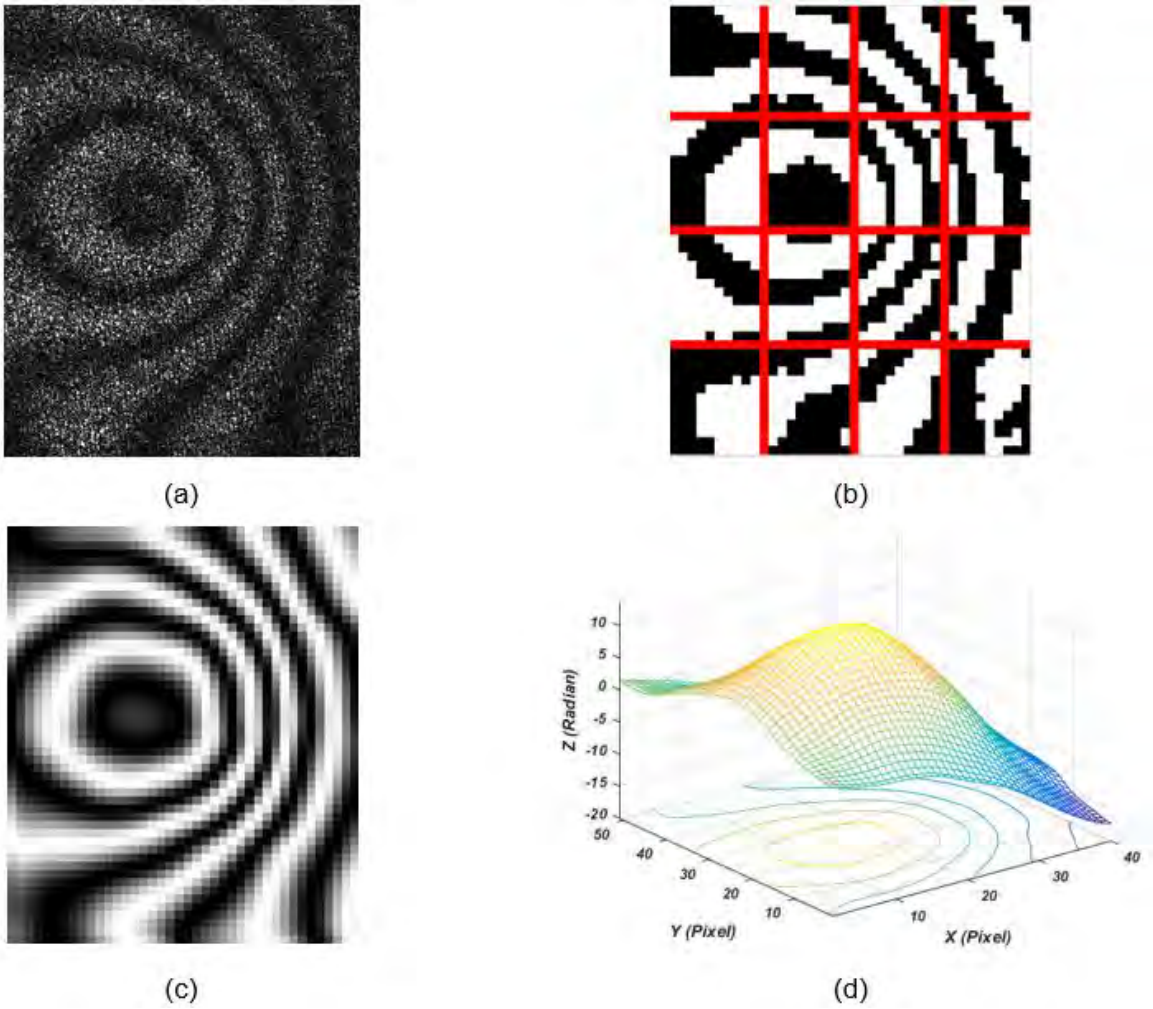

Fig. 5.11 Original interferogram with resolution of 390×307 pixels. b) Filtered and partitioned fringe pattern, recovered in low resolution. c) Recovered fringe pattern. d) Recovered phase map.

5.3 VMO using Bezier surface

Experimental tests were carried out to prove the effectiveness of the method, by means of a comparative analysis with computer simulated fringe patterns published in related works [45, 79, 46, 1]. The definition of VMO parameters was selected from an internal analysis presented in [76]. In all cases, the total expansion size used for these studies is $T = \frac{3}{2}N$, the vicinity (k) is 3, and the initial size of the population is ($N = 12$). The only parameters that were modified, depending on the complexity, were the number of evaluations of the fitness

function (C), the smoothness factor, and the dimension of the control mesh in their respective axes.

5.3.1 Computer simulated demodulated using Zernike polynomials

The proposed method was tested with a simulated image, which was demodulated using the bases of the Zernike polynomials to approximate the phase map of the object. This fringe pattern was taken from the experiments published by Mancilla [45](Figure 5.12-a). In this demodulation process, the control mesh was adjusted by a matrix of 4×4 points in each window, until reaching 2 000 generations of feasible solutions. The used smoothness factor was 5 units, and the time consumed to achieve convergence in each execution was 9 seconds. The resulting graphs obtained through this method are shown in Figure 5.12.

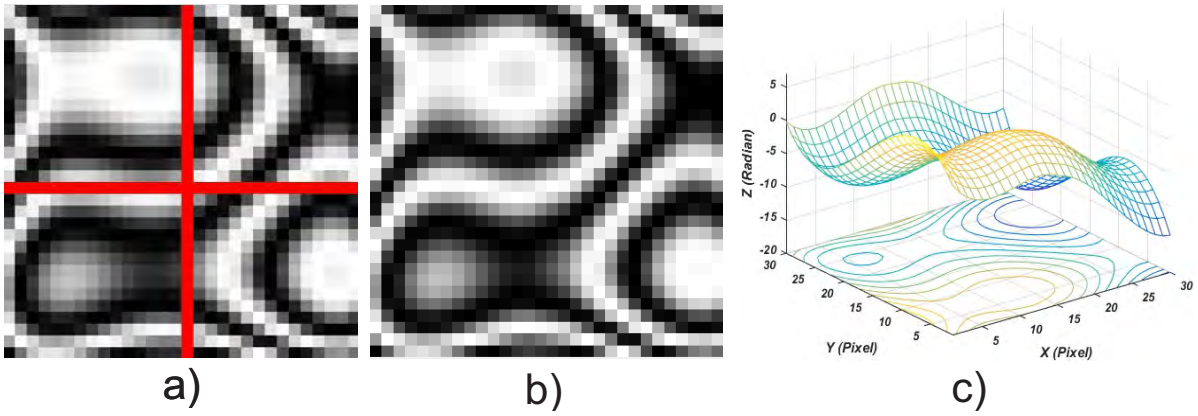

Fig. 5.12 a) Subdivided input pattern using a maximum number of window fringes equal to 4, with a resolution of 30×30 pixels. b) Fringe pattern, recovered by VMO method. c) Recovered phase map with an RMS value of 0.002661 rad.

5.3.2 Simulated pattern demodulated using a Particle Swarm Algorithm as optimization model

The fringe pattern used in this test was taken from the experiments published by Jimenez in [79] (Figure 5.13-d). This fringe pattern implemented a simple polynomial adjustment to

approximate the phase map of the object, using a Particle Swarm Algorithm as optimization model. In this demodulation process VMO parameters were the same as those used in Experiment 5.3.1. The resulting graphs obtained through this method are shown in Figure 5.13

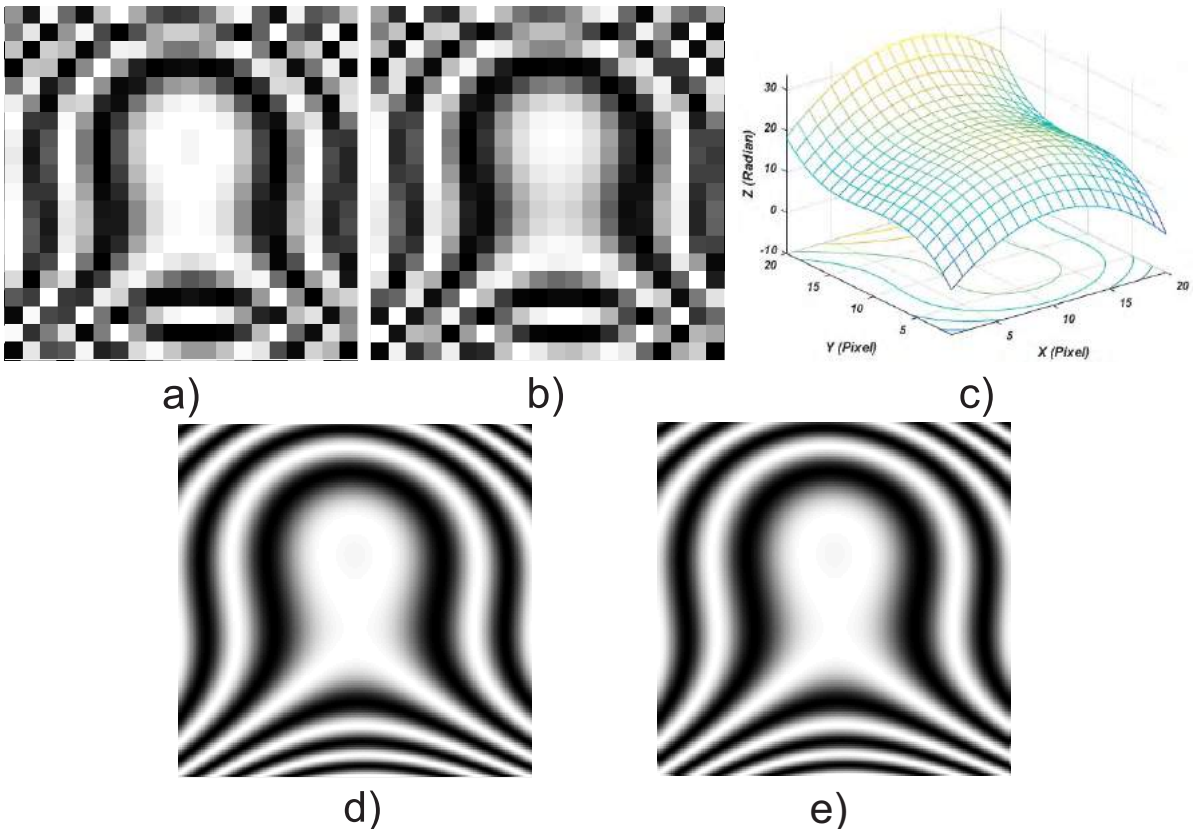

Fig. 5.13 a) Input fringe pattern, without applying automatic partitioning, with a resolution of 20×20 pixels. b) Fringe pattern generated during search process. c) Phase map recovered by the demodulation process, with an RMS error of 0.012316 rad. d) High-resolution simulated fringe pattern. e) Estimated fringe pattern by VMO, with a resolution of 250×250 pixels

5.3.3 Sub-sample fringe pattern

The following simulation is intended to demonstrate the ability of the algorithm to recover phase in low resolution fringe pattern, even when the Nyquist criterion is not met. The computer simulation corresponds to a fringe pattern presented in [1](Experiment 5.2.2), with

a resolution of 28×28 pixels. The result of applying the automatic partition method, with a maximum number of fringes per window of 6, is shown in Figure 5.14. Each window was

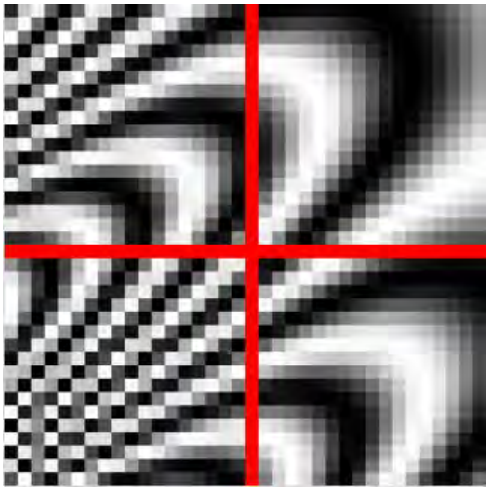

Fig. 5.14 Partitioned fringe pattern with a resolution of 28×28 pixels.

demodulated by adjusting a square matrix of 4×4 control points, up to 1000 evaluations of the fitness function, with a smoothness factor of 5 units, for a time of 5 seconds. The RMS error between the two phase maps was 0.00271 radians, improving the value of 0.0073 radians obtained in [1], and considerably decreasing the demodulation time; the results of the high-resolution demodulation process are shown in Figure 5.15.

5.3.4 Computer simulated proposed by Toledo and Cuevas

This experiment corresponds to the computer simulated fringe pattern presented in [46] (Experiment 5.2.3). A four-order control square matrix was used to approximate every window, the required stopping condition for VMO was 2 000 fitness function evaluations, the smoothness factor was $\mu = 10$, and the maximum number of fringes (F) used for automatic partitioning was $F = 5$. The results of the demodulation method are shown in Figure 5.16.

Taking into consideration the comparison of results presented in [1], the VMO method reduces the root mean squared (RMS) value of 0.007 rad obtained in [1] with a value of 0.002

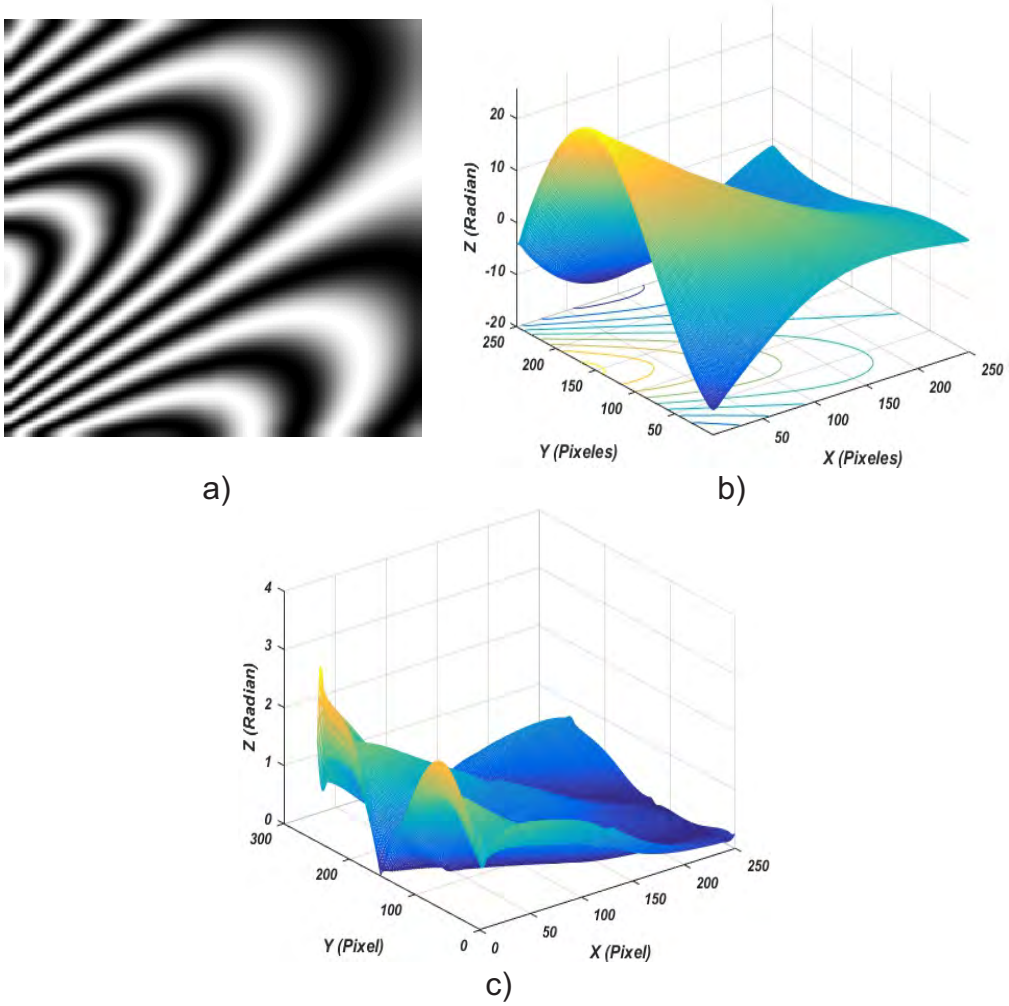

Fig. 5.15 a) VMO-recovered fringe pattern, with resolution of 250×250 pixels. b) High-resolution recovered phase map. c) Difference between original and demodulated phase.

rad. Another aspect to take into account is the speed of our model: it required 17 seconds to converge to a solution, lower than the 156 seconds achieved by Simulated Annealing (RS).

5.3.5 Digital holography interferometry proposed by Pramod Rastogi and Erwin Hackin

The next test corresponds to an experiment of Digital Holography Interferometry (DHI), which can be found in the book [24], by Pramod Rastogi and Erwin Hackin, in the chapter on Local Polynomial Phase Modeling and Estimation. As in [1], a low-pass filter was used

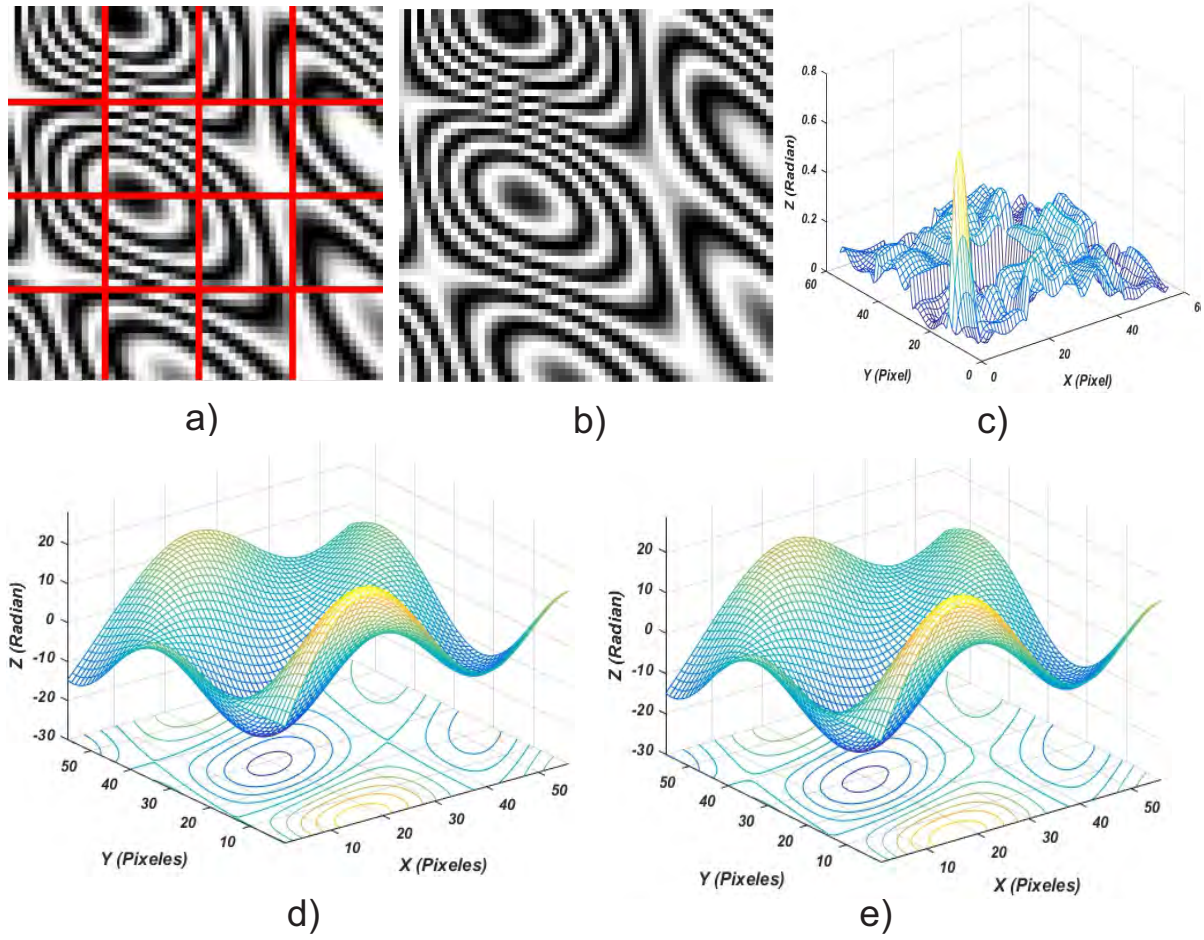

Fig. 5.16 a) Automatic partitioning of the original pattern. b) Recovered fringe pattern. c) Error between original and demodulated phase graphs. d) Simulated phase map. e) Phase map recovered by VMO method.

to remove noise and sub-sample the image, up to a resolution of 40×40 (Figure 5.17-b). The VMO method was applied over each window, through 4 000 fitness evaluations. The time consumed by the algorithm to obtain the complete phase map was only 18 seconds, using a squared control matrix of order 4, improving the 67 seconds reported in [1]. The results in the original resolution are shown in Figure 5.17-c,d.

5.3.6 Circularly clamped object

The next interferogram corresponds to the loading of a circularly clamped object, taken from [91]. After the pre-processing, the fringe pattern was partitioned into 4 separate windows,

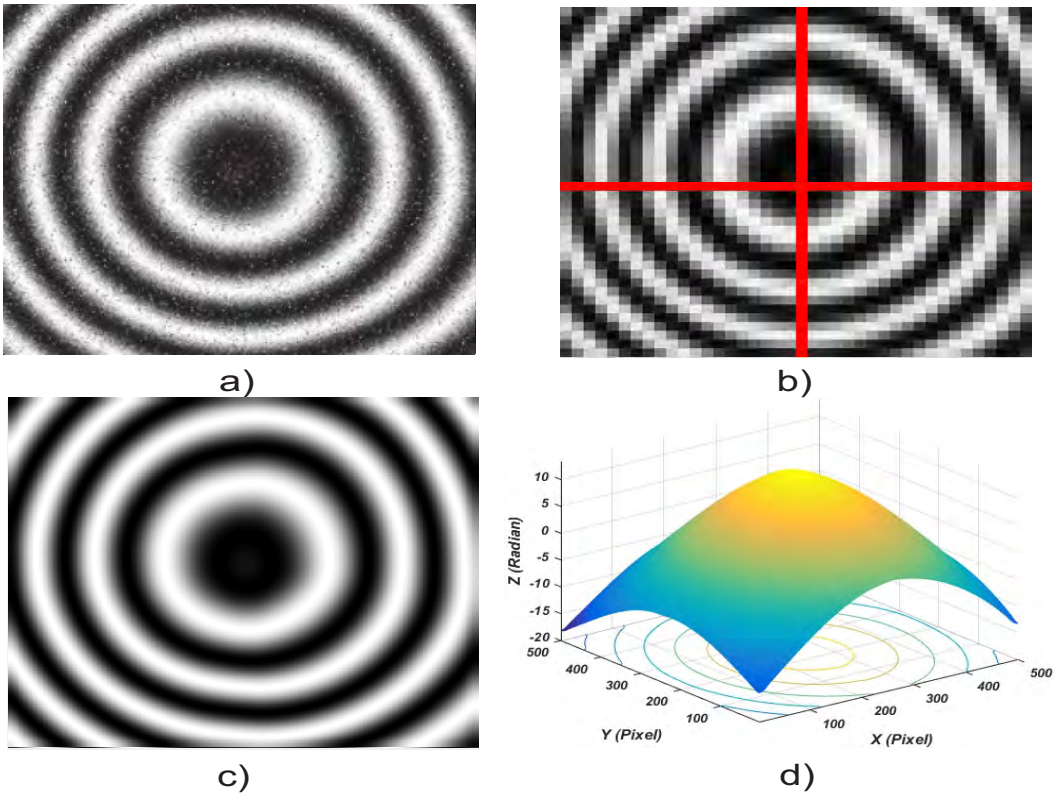

Fig. 5.17 a) Experimental fringe pattern with resolution of 500×500 pixels. b) Input fringe pattern after a noise removing, sub-sampling process, and automatic partitioning process. c) Fringe pattern recovered in high resolution. d) Phase map recovered in the original resolution.

and sampled to produce an image of 60×60 pixels to speed up the search process (Figure 5.18). Each partition was demodulated by adjusting a square control mesh of 4×4 elements, 8 000 evaluations of the fitness function, and a smoothness factor of 10, in order to obtain smoother solutions. The fringe pattern and the phase, estimated by VMO, were achieved in a time of 47 seconds. Figure 5.19 shows the results obtained during the demodulation process.

5.3.7 Comparison with Phase Shifting method

The last interferogram corresponds to a real shadow moire application, presented in [1]. This fringe pattern uses the phase shifting method to determine the three-dimensional surfaces to increase the accuracy of the shadow moire technique, in order to compare it with the proposed model. Figure 5.20 shows a sketch of the general experimental set up. The basic

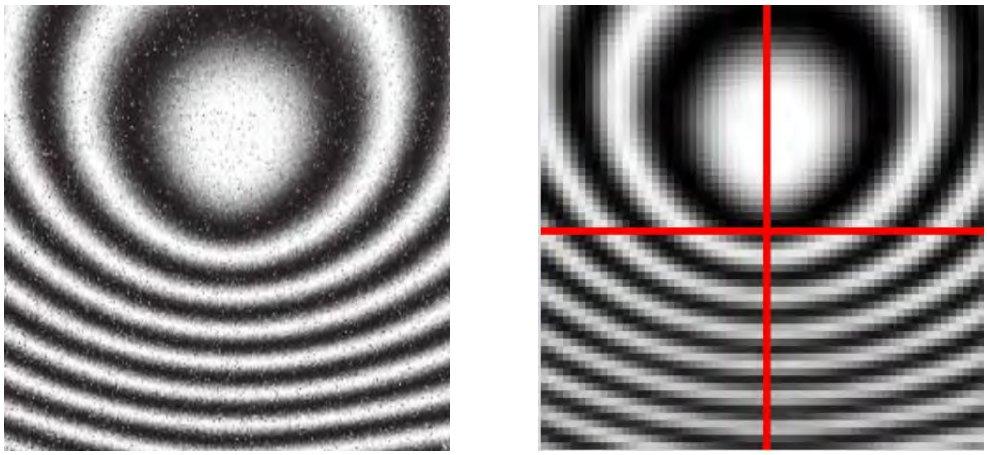

Fig. 5.18 a) Experimental fringe pattern. b) Filtered and sub-sampled fringe pattern, partitioned into 4 windows.

experimental arrangement consists of a white light source, a Ronchi grating, micrometer, and, usually, a CCD camera as observer.

A low-pass filter was applied to the fringe pattern obtained from the experimental arrangement to eliminate the high frequencies produced by the grid. Then it was reduced to a resolution of 35×41 pixels, and partitioned into windows with a maximum number of fringes equal to 7. Figure 5.21 shows the original interferogram obtained from the experimental set-up, and the partitioning fringe pattern, that is used as input for the presented model.

To achieve convergence, the VMO method required only 13 seconds, 2000 objective function evaluations, and a 4×4 element control mesh. The resulting graph obtained by this method and the comparison with Phase Shifting technique are presented in Figure 5.22.

5.4 Comparison of results

Comparing our methodology to other methods reported in the literature, using soft-computing techniques, our proposal presents an improvement in the quality of the results in terms of the approximation error and the execution time. Table 5.2 presents a comparison between the presented method and several methods that use a polynomial adjustment to obtain the phase

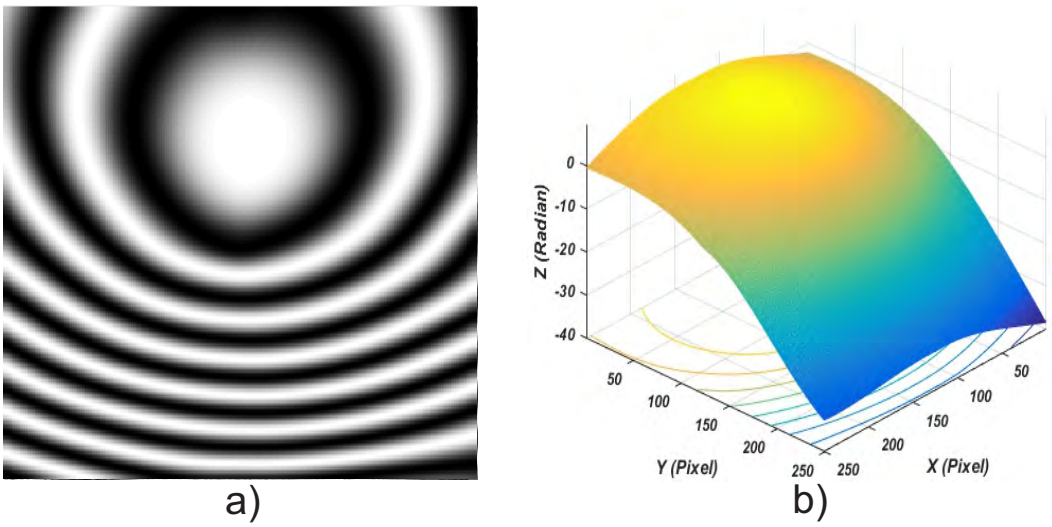

Fig. 5.19 a) Fringe pattern generated from the recovered phase, with a resolution of 250×250 pixels. b) Phase field obtained by VMO.

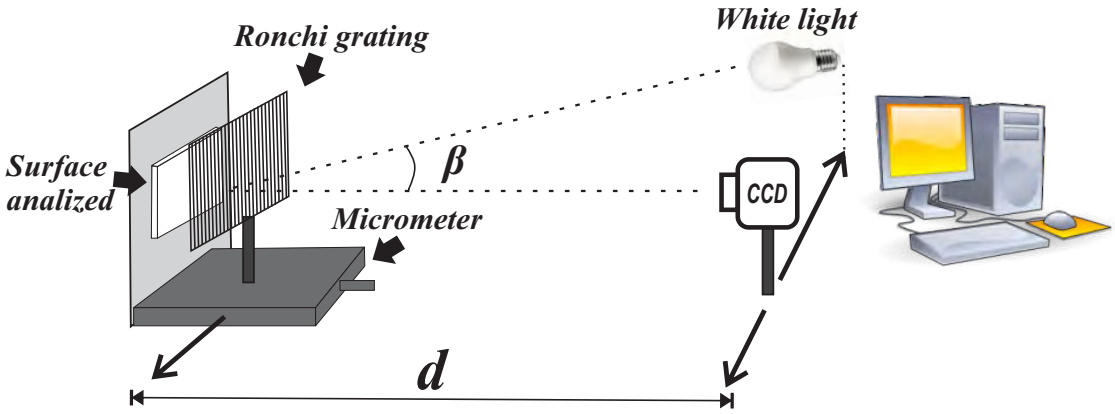

Fig. 5.20 Shadow moire basic experimental arrangement.

field (Parallel Demodulation using Simulated Annealing (SA) [1] and Independent Windows, using Genetic Algorithm (AG) [46]). In order to obtain a more transparent comparison, two groups of experimental tests were made, using equal conditions; group 1 was tested in a computer with a Windows 10 Professional (64 bits) operating system. The processor used was an AMD Ryzen 7 3700U, running at 2.3 GHz, with a remote access memory (RAM) of 20.0 GB, and the group 2 used the same hardware resource as in the experimental section. In this comparison 2 metrics were added Mean Squared Error (MSE) and the Fringe error (Fe), the latter metric was introduced to determine the similarity, mainly in the real experiments. The MSE is a measure of the quality of an estimator which measures the average of the

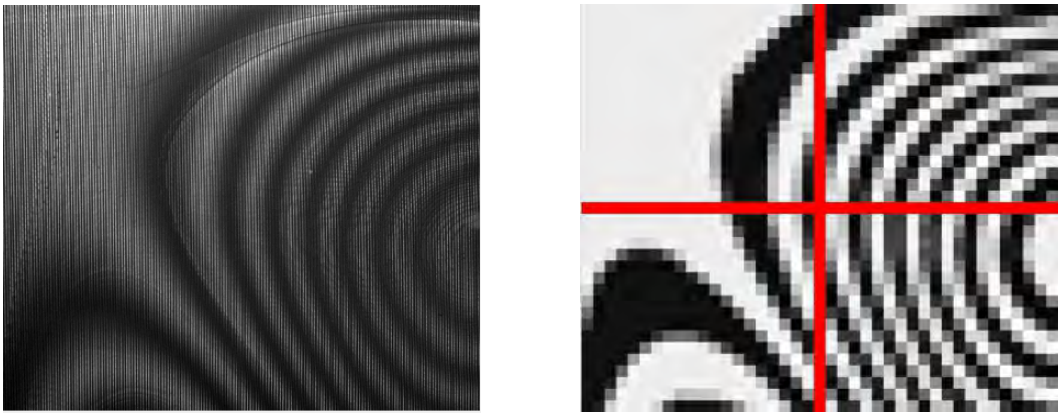

Fig. 5.21 a) Original shadow Moire fringe pattern, with resolution of 831×971 pixels. b) Partitioned input fringe pattern, with a maximum number of fringe equal to 7.

squares of the errors that is, the average squared difference between the estimated values and the actual value, the MSE is computed as:

$$MSE = \frac{1}{RC} \sum_{i=0}^{C-1} \sum_{j=0}^{R-1} ||f(x,y) - \phi(x,y)||^2, \tag{5.4}$$

where R and C correspond to the number of rows and columns of the fringe pattern, f and ϕ define the original phase map and the one recovered by the model, respectively.

Fe is the equivalent of the mean absolute error (MAE), which is a measure of the difference between the original and the VMO recovered fringe pattern. This metric can be defined by the following equation:

$$F_e = \frac{1}{CR} \sum_{i=0}^{C-1} \sum_{j=0}^{C-1} ||f(x,y) - \phi(x,y)||, \tag{5.5}$$

where R and C are the fringe pattern resolutions, I is the original interferogram, and I_R corresponds to fringe pattern recovered by VMO. In all cases, VMO shows improvement in terms of the approximation error and convergence time.

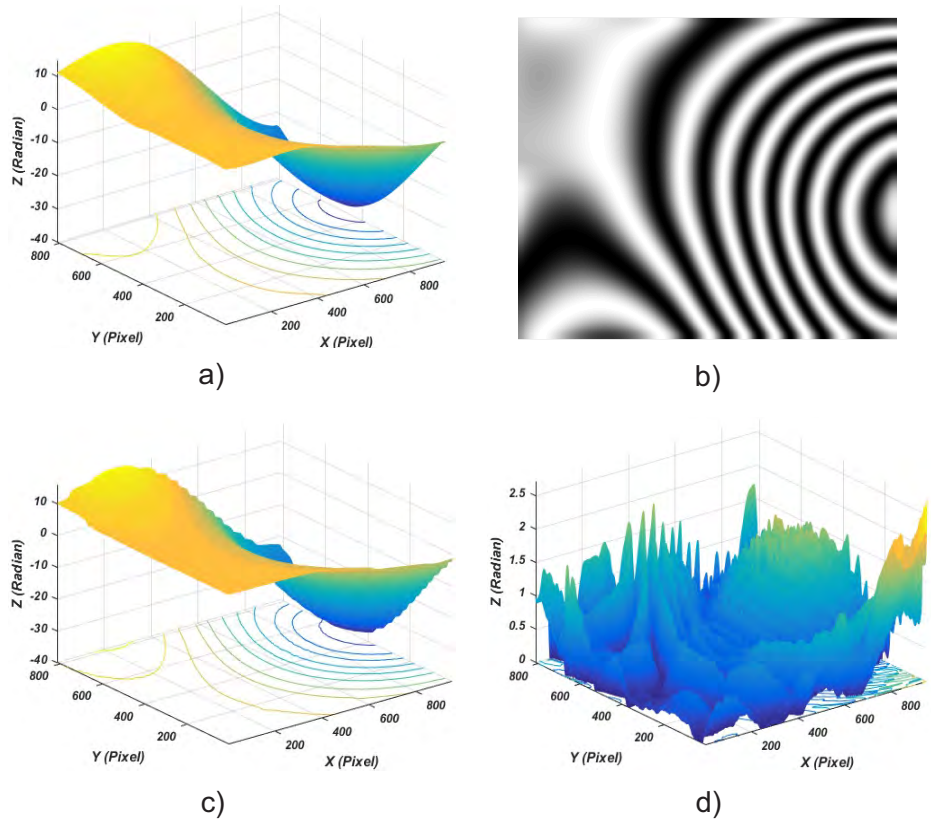

Fig. 5.22 a) Phase map recovered by VMO in the original resolution. b) Fringe pattern generated from the approximated phase field. c) Phase map obtained by Phase Shifting method. d) Error difference between phase shifting and demodulated phase with an RMS value of 7.3353×10^{-4} radians.

Table 5.2 Comparison of results with different methods using an optimization model.

	Experiment	Method	RMS (radians)	MSE (radians)	Fringe Error (Fe)	Time (seconds)
Group 1 Simulated fringe patterns	5.2.3	VMO	0.0024	0.0189	9.3108	36
		SA	0.0070	0.1626	27.7371	216
		AG	0.1540	74.3734	43.8800	412
	5.3.1	VMO	0.0026	0.0088	6.4396	14
		SA	0.0360	1.6796	36.6531	63
		AG	0.0772	7.7240	57.2700	98
	5.3.2	VMO	0.0123	0.0605	15.5040	8
		SA	0.0597	1.4256	38.4529	23
		AG	0.0594	1.4113	44.4900	34
Group 2 Real fringe patterns	5.3.4	VMO	—	—	16.5745	18
		SA	—	—	25.5505	67
	5.3.5	VMO	—	—	17.2883	47
		SA	—	—	42.3741	218

Chapter 6

Conclusions and Future Works

6.1 Conclusions

In the present doctoral thesis work, a study and review of the main conventional fringe demodulation techniques, i.e. Phase-Shifting, Fourier methods, and Regularized Phase Tracing, was carried out. Phase-shifting is a powerful technique used in optical metrology to measure a wide variety of physical quantities; unfortunately, this algorithm requires at least three interferograms with known phase shifts. This requirement may be unpractical in certain experiments, such as transient mechanical processes, or in testing with acquisition of multiple undisturbed interferograms. Fourier transform is a global method that can recover the phase from a single interferogram, but has the disadvantage that it only analyzes patterns of open fringes, and usually, the global phase is too complex to be mathematically represented. Moreover, this method and Phase-Shifting estimate the wrapped phase because of the arctangent function used in the phase computation, and consequently, it needs a phase development algorithm, in addition to requiring the design of a filter, to obtain the phase. On the other hand, Regularized Phase Tracing is one of the most robust and effective methods, although it often fails in the cases of complex interferograms, and needs well-defined scanning strategies.

As a result of this research it was shown that the population metaheuristic Variable Mesh Optimization, and the optimization algorithm known as Simulated Annealing can be modeled

as a problem for interferogram demodulation. A technique based on parallel demodulation was proposed for demodulating a single interferogram using SA. This model establishes a new design to partition the interferogram automatically, using a recursive method that stores in a quad tree data structure, the subimages with a limit of fringes in each partition. This partition allows to reduce the complexity of the windows and makes the search of the algorithm of optimization more viable. In addition, it improves the window unification method when using cubic tracing mediating approaches. Consequently, this will lead to the elimination of overlapping regions and thus avoid multiple demodulation of border regions. Another advantage offered by the model is that, by finding an approximation through polynomial functions, and at the end of the method, it is possible to recover its original size through the approximation function.

As a second part of this project, several changes were introduced in order to obtain consistent, improvements in terms of quality of the demodulation process and execution time. A robust technique for single interferogram demodulation, based on the concept of parallel demodulation has been proposed. This model establishes a novel methodology employing Bezier surfaces to fit the phase map, and estimates the control mesh employing a global optimization algorithm, i.e., variable mesh optimization.

Bezier surfaces revolutionize polynomial-based phase fitting, in the sense that due to the usefulness of their properties, it is possible to split the search of the algorithm towards the edges of the fringe pattern and towards the central region. In addition, similar to the methods based on a polynomial adjustment, the proposed does not require the use a phase development algorithm, because the model itself is based directly on the phase map and does not involve the cosine function. Furthermore, it can sub-sample the interferogram to speed up the search and finally recover the original size from a simple scaling. Although the main limitation of demodulation methods using an optimization model is with respect to the configuration of the algorithm parameters, it may be concluded that VMO offered stability in selecting them, which explains why it was possible to establish the same configuration for all the test functions, where the only modifiable value was the stopping condition, which is linked to the complexity of the pattern. At the same time, we present experimental results on the capacity

of approximation and the decrease in demodulation time, in comparison with other methods in literature.

Finally, this work demonstrates the demodulation capacity, even though the resolution of fringe pattern does not satisfy the Nysquit criterion, and confirms the capability of Bezier surfaces in computer-aided design.

6.2 Future Works

Today one of the main challenges of engineering is to obtain an accurate measurement, especially in transient events, where it is very difficult to record a measurement. That is why one of the challenges in Optical Metrology is to find the phase map from a real time interferogram. One of the motivations consists in the design and implementation of an application at the hardware level in such a way that it can deliver real-time measurements, using Graphical Processing Units (GPUs). This type of technology, designed for parallel computing, is ideal for the demodulation principle developed in the thesis project. This principle is based on dividing a large problem into a set of several small problems that can be solved by GPU technology, which can facilitate a real-time application.

Another line of future research would be the use of a priori knowledge of the problem. In many situations we have an idea of the shape of the object in question, which is why we could take advantage of the particularities of Bezier surfaces, which describe an envelope surrounding the shape of the object, so that we would have a starting point in the population, which would considerably facilitate the process of searching for an optimization algorithm. It is not less certain that this technique represent a novelty in this type of problem, which is why another line of future research would be the comparison and implementation of different metaheuristics, using Bezier surfaces for the parametric adjustment of the phase map. With this process it is possible to perform a thorough analysis and conclude on which optimization model fits this type of approach.

Finally, by taking advantage of the properties of Bezier surfaces, it is possible to eliminate or facilitate the process of unifying windows by partitioning where neighboring windows share

an overlapping row or column. With this, a linear demodulation process could be carried out on the overlapping regions, and then an adjustment could be made to eliminate the height differences between the edges of the windows. This process would have the advantage that it would not be necessary to use any type of extrapolation in the process of unification, in addition to the fact that sharing the same edge guarantees that the bonding is perfect.

6.3 Works relate to the thesis

Congress

- First Congress of Engineering in Computer Systems and Applications (CISCA), Simulated Annealing for Demodulation of Fringe Patterns,I. Moré and F. Cuevas, November 2017, Puebla, México.
- The International Symposium on Optomechatronic Technology, Fringe Demodulation using Simulated Annealing with Independent Window Partition, I. More, F. Cuevas, November 2018, Cancún, México.
- The Iberoamerican Optics Meeting and the Latinamerican Meeting on Optics, Lasers and Applications (RIAO-OPTILAS), Simulated Annealing applied to interferogram demodulation based on the independent window technique, I. More, F. Cuevas, September 2019, Cancún, México.

Publications

- **I. Moré, F. Cuevas, J. Jiménez** "Parallel demodulation algorithm for processing independent windows of a fringe patterns using simulating annealing", Optics Communications, vol. 463, p. 125403, 2020.
- **I. Moré, F. Cuevas, J. Jiménez, A. Puris, F. Sosa** "Variable mesh optimization applied to fringe patterns demodulation using a Bézier surface", Applied Optics, Vol. 60, No. 24, August 2021

References

[1] "Parallel demodulation algorithm for processing independent windows of a fringe patterns using simulating annealing," *Optics Communications*, vol. 463, p. 125403, 2020.

[2] D. Li, C. Liu, and J. Tian, "Telecentric 3d profilometry based on phase-shifting fringe projection," *Optics Express*, vol. 22, pp. 31826–31835, Dec 2014.

[3] J. Salvi, S. Fernandez, T. Pribanic, and X. Llado, "A state of the art in structured light patterns for surface profilometry," *Pattern Recognition*, vol. 43, no. 8, pp. 2666–2680, 2010.

[4] F. Chen, G. M. Brown, and M. Song, "Overview of 3-D shape measurement using optical methods," *Optical Engineering*, vol. 39, no. 1, pp. 10 – 22, 2000.

[5] R. Klette, K. Schluns, and A. Koschan, *Computer Vision: Three-Dimensional Data from Images*. Springer Singapore, 1996.

[6] B. K. Horn, *Robot Vision*. Mc Graw Hill, 1986.

[7] H. Zhao, H. Du, J. Li, and Y. Qin, "Shadow moire technology based fast method for the measurement of surface topography," *Applied Optics*, vol. 52, pp. 7874–7881, Nov 2013.

[8] G. Mauvoisin, F. Brémand, and A. Lagarde, "Three-dimensional shape reconstruction by phase-shifting shadow moiré," *Applied Optics*, vol. 33, pp. 2163–2169, Apr 1994.

[9] S. Van der Jeught and J. J. Dirckx, "Real-time structured light profilometry: a review," *Optics and Lasers in Engineering*, vol. 87, pp. 18–31, 2016.

[10] J. Huang and Q. Wu, "A new reconstruction method based on fringe projection of three-dimensional measuring system," *Optics and Lasers in Engineering*, vol. 52, pp. 115–122, 2014.

[11] L. Huang, Q. Kemao, B. Pan, and A. K. Asundi, "Comparison of fourier transform, windowed fourier transform, and wavelet transform methods for phase extraction from a single fringe pattern in fringe projection profilometry," *Optics and Lasers in Engineering*, vol. 48, no. 2, pp. 141–148, 2010.

[12] D. E. Goldberg, *Genetic Algorithms in Search, Optimization and Machine Learning*. Boston, MA, USA: Addison-Wesley Longman Publishing Co., Inc., 1st ed., 1989.

[13] E.-G. Talbi, *Metaheuristics: From Design to Implementation*. Wiley Publishing, 2009.

[14] T. Bäck, *Evolutionary Algorithms in Theory and Practice: Evolution Strategies, Evolutionary Programming, Genetic Algorithms*. USA: Oxford University Press, Inc., 1996.

[15] M. Servin, J. L. Marroquin, and F. J. Cuevas, "Demodulation of a single interferogram by use of a two-dimensional regularized phase-tracking technique," *Applied Optics*, vol. 36, pp. 4540–4548, Jul 1997.

[16] T. Back, D. B. Fogel, and Z. Michalewicz, *Handbook of Evolutionary Computation*. GBR: IOP Publishing Ltd., 1st ed., 1997.

[17] C. Blum, J. Puchinger, G. R. Raidl, and A. Roli, "Hybrid metaheuristics in combinatorial optimization: A survey," *Applied Soft Computing*, vol. 11, no. 6, pp. 4135–4151, 2011.

[18] E. De Mendonça Mesquita, R. C. Sampaio, H. V. H. Ayala, and C. H. Llanos, "Recent meta-heuristics improved by self-adaptation applied to nonlinear model-based predictive control," *IEEE Access*, vol. 8, pp. 118841–118852, 2020.

[19] N. Akbarpour, M. Hajiaghaei-Keshteli, and R. Tavakkoli-Moghaddam, "New approaches in meta-heuristics to schedule purposeful inspections of workshops in manufacturing supply chains," *International Journal of Engineering*, vol. 33, no. 5, pp. 833–840, 2020.

[20] A. Gogna and A. Tayal, "Metaheuristics: review and application," *Journal of Experimental & Theoretical Artificial Intelligence*, vol. 25, no. 4, pp. 503–526, 2013.

[21] H. Schwenke, U. Neuschaefer-Rube, T. Pfeifer, and H. Kunzmann, "Optical methods for dimensional metrology in production engineering," *CIRP Annals*, vol. 51, no. 2, pp. 685 – 699, 2002.

[22] G. Mauvoisin, F. J. Bremand, and A. Lagarde, "Shadow moire by phase shifting method and applications," in *Optics, Illumination, and Image Sensing for Machine Vision VIII* (D. J. Svetkoff, ed.), vol. 2065, pp. 170 – 181, International Society for Optics and Photonics, SPIE, 1994.

[23] P. K. Rastogi, *Digital Speckle Pattern Interferometry and Related Techniques*. 2000.

[24] P. Rastogi and E. Hack, *Phase Estimation in Optical Interferometry*. Taylor & Francis, 2014.

[25] U. Schnars and W. P. O. Jüptner, "Digital recording and reconstruction of holograms in hologram interferometry and shearography," *Applied Optics*, vol. 33, pp. 4373–4377, Jul 1994.

[26] L. Salas, E. Luna, J. Salinas, V. M. Garcia, and M. Servin, "Profilometry by fringe projection," *Optical Engineering*, vol. 42, no. 11, pp. 3307 – 3314, 2003.

[27] S. Ajithaprasad and R. Gannavarpu, "Non-invasive precision metrology using diffraction phase microscopy and space-frequency method," *Optics and Lasers in Engineering*, vol. 109, pp. 17 – 22, 2018.

[28] E. Robin, V. Valle, and F. Brémand, "Phase demodulation method from a single fringe pattern based on correlation with a polynomial form," *Applied Optics*, vol. 44, pp. 7261–7269, Dec 2005.

[29] M. Rivera, "Robust phase demodulation of interferograms with open or closed fringes," *Journal of the Optical Society of America A*, vol. 22, pp. 1170–1175, Jun 2005.

[30] J. C. Estrada, M. Servin, and J. L. Marroquín, "Local adaptable quadrature filters to demodulate single fringe patterns with closed fringes.," *Optics Express*, vol. 15, pp. 2288–2298, Mar 2007.

[31] Q. Kemao and S. H. Soon, "Sequential demodulation of a single fringe pattern guided by local frequencies," *Optics Letters*, vol. 32, pp. 127–129, Jan 2007.

[32] O. D. Cedeño, M. Rivera, and R. Legarda-Saenz, "Fast phase recovery from a single closed-fringe pattern," *Journal of the Optical Society of America A*, vol. 25, pp. 1361–1370, Jun 2008.

[33] Z. Dong and H. Cheng, "Hybrid algorithm for phase retrieval from a single spatial carrier fringe pattern," *Applied Optics*, vol. 55, pp. 7565–7573, Sep 2016.

[34] M. Trusiak, Ł. Służewski, and K. Patorski, "Single shot fringe pattern phase demodulation using hilbert-huang transform aided by the principal component analysis," *Optics Express*, vol. 24, pp. 4221–4238, Feb 2016.

[35] S. Feng, Q. Chen, G. Gu, T. Tao, L. Zhang, Y. Hu, W. Yin, and C. Zuo, "Fringe pattern analysis using deep learning," *Advanced Photonics*, vol. 1, no. 2, pp. 1 – 7 – 7, 2019.

[36] W. Jinmin, L. Mingfeng, J. Chenchen, L. Pei-Hang, Z. Feng, and T. Ran, "Fractional fourier ridges for demodulation of interferograms with quadratic phase," p. 2, 06 2019.

[37] A. Collaro, G. Franceschetti, F. Palmieri, and M. S. Ferreiro, "Phase unwrapping by means of genetic algorithms," *Journal of the Optical Society of America A*, vol. 15, pp. 407–418, Feb 1998.

[38] F. J. Cuevas, J. H. Sossa-Azuela, and M. Servin, "A parametric method applied to phase recovery from a fringe pattern based on a genetic algorithm," *Optics Communications*, vol. 203, no. 3-6, pp. 213–223, 2002.

[39] S. Vázquez-Montiel, J. J. Sánchez-Escobar, and O. Fuentes, "Obtaining the phase of an interferogram by use of an evolution strategy: Part i.," *Applied Optics*, vol. 41, pp. 3448–3452, Jun 2002.

[40] D. Malacara, "Interferogram evaluation and wavefront fitting," *Optical shop testing*, 1992.

[41] J. J. Sánchez-Escobar and L. I. B. Santillán, "Experimental interferogram analysis using an evolutionary local search algorithm," in *Optical Design and Fabrication 2017 (Freeform, IODC, OFT)*, p. JTu5A.29, Optical Society of America, 2017.

[42] F. J. Cuevas, F. Mendoza, M. Servin, and J. H. Sossa-Azuela, "Window fringe pattern demodulation by multi-functional fitting using a genetic algorithm," *Optics Communications*, vol. 261, no. 2, pp. 231–239, 2006.

[43] O. G. Angelez, "Demodulación de patrones de franjas cerradas mediante un algoritmo genético," Master's thesis, Instituto Tecnologico de Leon, Leon, Guanajuato, Mexico, 2005.

[44] O. D. Cedeño, "Algoritmo rápido para recuperar fase de un solo interferograma con franjas abiertas y cerradas," Master's thesis, Centro de Investigación en Matemáticas A.C., Guanajuato, Mexico, 2006.

[45] L. Espinosa, J. Valadez, and F. Cuevas, "Demodulation of interferograms of closed fringes by zernike polynomials using a technique of soft computing," *Engineering Letters*, vol. 15, 08 2007.

[46] L. E. Toledo and F. J. Cuevas, "Optical metrology by fringe processing on independent windows using a genetic algorithm," *Experimental Mechanics*, vol. 48, no. 4, pp. 559–569, 2008.

[47] J. F. Jimenez, F. J. Cuevas, J. H. Sossa, and L. E. Gomez, "A parametric method applied to phase recovery from a fringe pattern based on a particle swarm optimization," in *Hybrid Artificial Intelligence Systems* (M. Graña Romay, E. Corchado, and M. T. Garcia Sebastian, eds.), (Berlin, Heidelberg), pp. 40–47, Springer Berlin Heidelberg, 2010.

[48] U. Rodríguez, M. Mora-González, J. Muñoz-Maciel, and T. Ramírez del Real, "Fsd-hso optimization algorithm for closed fringes interferogram demodulation," *Mathematical Problems in Engineering*, vol. 2016, pp. 1–11, 03 2016.

[49] D. Robinson and G. Reid, *Interferogram Analysis, Digital Fringe Pattern Measurement Techniques*. Taylor & Francis, 1993.

[50] M. Takeda, H. Ina, and S. Kobayashi, "Fourier-transform method of fringe-pattern analysis for computer-based topography and interferometry," *Journal of the Optical Society of America A*, vol. 72, pp. 156–160, Jan 1982.

[51] M. Takeda and K. Mutoh, "Fourier transform profilometry for the automatic measurement of 3-d object shapes," *Applied Optics*, vol. 22, pp. 3977–3982, Dec 1983.

[52] D. Malacara, *Optical shop testing*, vol. 59. John Wiley & Sons, 2007.

[53] M. Kujawinska and J. Wojciak, "Spatial-carrier phase-shifting technique of fringe pattern analysis," in *Industrial Applications of Holographic and Speckle Measuring Techniques* (W. P. O. Jueptner, ed.), vol. 1508, pp. 61 – 67, International Society for Optics and Photonics, SPIE, 1991.

[54] E. Hecht, *Optica*. Estados Unidos:Addison-Wesley, 1986.

[55] M. Servín, J. A. Quiroga, and M. Padilla, *Fringe pattern analysis for optical metrology: theory, algorithms, and applications*. John Wiley & Sons, 2014.

[56] J. Morlet, *Sampling Theory and Wave Propagation*, pp. 233–261. Berlin, Heidelberg: Springer Berlin Heidelberg, 1983.

[57] Q. Kemao, *Windowed fringe pattern analysis*. 2013.

[58] C. Joenathan and B. Khorana, "Phase measurement by differentiating interferometric fringes," *Journal of Modern Optics*, vol. 39, no. 10, pp. 2075–2087, 1992.

[59] W. Nadeborn, P. Andrä, and W. Osten, "A robust procedure for absolute phase measurement," *Optics and Lasers in Engineering*, vol. 24, no. 2, pp. 245–260, 1996. Civil and Structural Engineering Measurements with Interferometry, Shearography, and Holography.

[60] P. Carré, "Installation et utilisation du comparateur photoélectrique et interférentiel du bureau international des poids et mesures," *Metrologia*, vol. 2, pp. 13–23, jan 1966.

[61] R. Crane, "Interference phase measurement," *Applied Optics*, vol. 8,3, p. 345, 1969.

[62] J. H. Bruning, D. R. Herriott, J. E. Gallagher, D. P. Rosenfeld, A. D. White, and D. J. Brangaccio, "Digital wavefront measuring interferometer for testing optical surfaces and lenses," *Applied Optics*, vol. 13, pp. 2693–2703, Nov 1974.

[63] J. W. Hardy, J. E. Lefebvre, and C. L. Koliopoulos, "Real-time atmospheric compensation," *Journal of the Optical Society of America A*, vol. 67, pp. 360–369, Mar 1977.

[64] J. H. Bruning, *Fringe Scanning Interferometers*, p. 409. 1978.

[65] P. Hariharan, *Basics of Interferometry*. Elsevier Science, 2010.

[66] J. Min, B. Yao, P. Gao, R. Guo, J. Zheng, and T. Ye, "Parallel phase-shifting interferometry based on michelson-like architecture," *Applied Optics*, vol. 49, pp. 6612–6616, Dec 2010.

[67] D. G. Abdelsalam, B. Yao, P. Gao, J. Min, and R. Guo, "Single-shot parallel four-step phase shifting using on-axis fizeau interferometry," *Applied Optics*, vol. 51, pp. 4891–4895, Jul 2012.

[68] N.-I. Toto-Arellano, D.-I. Serrano-García, and A. Martínez-García, "Parallel two-step phase shifting interferometry using a double cyclic shear interferometer," *Optics Express*, vol. 21, pp. 31983–31989, Dec 2013.

[69] X. Su and W. Chen, "Reliability-guided phase unwrapping algorithm: a review," *Optics and Lasers in Engineering*, vol. 42, no. 3, pp. 245–261, 2004.

[70] F. Glover, "Future paths for integer programming and links to artificial intelligence," *Computers Operations Research*, vol. 13, no. 5, pp. 533–549, 1986. Applications of Integer Programming.

[71] F. Glover and G. Kochenberger, *Handbook of Metaheuristics*. International Series in Operations Research & Management Science, Springer US, 2003.

[72] M. R. Garey and D. S. Johnson, *Computers and Intractability; A Guide to the Theory of NP-Completeness*. USA: W. H. Freeman Co., 1990.

[73] M. Yagiura and T. Ibaraki, "On metaheuristic algorithms for combinatorial optimization problems," *Systems and Computers in Japan*, vol. 32, no. 3, pp. 33–55, 2001.

[74] S. Kirkpatrick, C. D. Gelatt, and M. P. Vecchi, "Optimization by Simulated Annealing," *American Association for the Advancement of Science*, vol. 220, no. 4598, pp. 671–680, 1983.

[75] N. Metropolis, A. Rosenbluth, M. Rosenbluth, A. Teller, and E. Teller, "Equation of State Calculations by Fast Computing Machines," *The Journal of Chemical Physics*, vol. 21, pp. 1087–1092, 1953.

[76] A. Puris, R. Bello, D. Molina, and F. Herrera, "Variable mesh optimization for continuous optimization problems," *Soft Computing*, vol. 16, no. 5, pp. 511–525, 2012.

[77] F. Cuevas, M. Servin, and R. Rodriguez-Vera, "Depth object recovery using radial basis functions," *Optics Communications*, vol. 163, no. 4, pp. 270 – 277, 1999.

[78] F. Cuevas, M. Servin, O. Stavroudis, and R. Rodriguez-Vera, "Multi-layer neural network applied to phase and depth recovery from fringe patterns," *Optics Communications*, vol. 181, no. 4, pp. 239 – 259, 2000.

[79] J. Jiménez, H. Sossa, F. Cuevas, and L. Gómez, "Demodulation of Interferograms based on Particle Swarm Optimization," *Polibits*, pp. 83 – 91, 06 2012.

[80] M. Goodrich, R. Tamassia, and D. Mount, *Data Structures and Algorithms in C++*. Wiley, 2004.

[81] P. Moscato, "An Introduction to Population Approaches for Optimization and Hierarchical Objective Functions: A Discussion on the Role of Tabu Search," *Ann. Oper. Res.*, vol. 41, pp. 85–121, may 1993.

[82] M. F. Cardoso, R. L. Salcedo, S. F. De Azevedo, and et. al., "Nonequilibrium simulated annealing: a faster approach to combinatorial minimization," *Industrial and Engineering Chemistry Research*, vol. 33, p. 1908, 1994.

[83] Y. Nourani and B. Andresen, "A comparison of simulated annealing cooling strategies," *Journal of Physics A: Mathematical and General*, vol. 31, no. 41, p. 8373, 1998.

[84] R. Burden and J. Faires, *Análisis numérico*. International Thomson Editores, 2002.

[85] S. Bernstein, "Démonstration du théoréme de weierstrass fondée sur le calcul des probabilités," *Communications de la Société Mathématique de Kharkov 2*, no. Series XIII No. 1, pp. 1–2, 1912.

[86] I. N. Bernshtein, "Modules over a ring of differential operators. study of the fundamental solutions of equations with constant coefficients," *Functional Analysis and Its Applications*, vol. 5, 1971.

[87] M. Sato and T. Shintani, "On zeta functions associated with prehomogeneous vector spaces," *Annals of Mathematics*, vol. 100, no. 1, pp. 131–170, 1974.

[88] D. Rogers, J. Adams, and J. Adams, *Mathematical Elements for Computer Graphics*. McGraw-Hill, 1976.

[89] I. Moré, F. Cuevas, J. Jimenez, A. Puris, and F. Sosa, "Variable mesh optimization applied to fringe pattern demodulation using a bézier surface," *Appl. Opt.*, vol. 60, pp. 7351–7361, Aug 2021.

[90] N. Otsu, "A Threshold Selection Method from Gray-level Histograms," *IEEE Transactions on Systems, Man and Cybernetics*, vol. 9, no. 1, pp. 62–66, 1979.

[91] S. S. Gorthi and P. Rastogi, "Windowed high-order ambiguity function method for fringe analysis," *The Review of scientific instruments*, vol. 80, no. 7, 2009.